

An updated Gamma Ray Bursts Hubble diagram

V.F. Cardone^{1,2}, S. Capozziello^{1,3}, M.G. Dainotti^{4,5,6}

¹ *Dipartimento di Scienze Fisiche, Università di Napoli "Federico II", Complesso Universitario di Monte Sant' Angelo, Edificio N, via Cinthia, 80126 - Napoli, Italy*

² *Dipartimento di Fisica Generale, Università di Torino, and I.N.F.N. - Sez. di Torino, Via Pietro Giuria 1, 10125 - Torino, Italy*

³ *I.N.F.N., Sez. di Napoli, Complesso Universitario di Monte Sant' Angelo, Edificio G, via Cinthia, 80126 - Napoli, Italy*

⁴ *ICRANet and ICRA, Piazzale della Repubblica 10, 65122 - Pescara, Italy*

⁵ *Dipartimento di Fisica, Università di Roma "La Sapienza", Piazzale Aldo Moro 5, 00185 - Roma, Italy*

⁶ *Observatorium Astronomiczne, Uniwersytet Jagiellonski, ul. Orła 175 - 31-501 Krakow, Poland*

Accepted xxx, Received yyy, in original form zzz

ABSTRACT

Gamma ray bursts (GRBs) have recently attracted much attention as a possible way to extend the Hubble diagram to very high redshift. To this aim, the luminosity (or isotropic emitted energy) of a GRB at redshift z must be evaluated from a correlation with a distance independent quantity so that one can then solve for the luminosity distance $D_L(z)$ and hence the distance modulus $\mu(z)$. Averaging over five different two parameters correlations and using a fiducial cosmological model to calibrate them, Schaefer (2007) has compiled a sample of 69 GRBs with measured $\mu(z)$ which has since then been widely used to constrain cosmological parameters. We update here that sample by many aspects. First, we add a recently found correlation for the X-ray afterglow and use a Bayesian inspired fitting method to calibrate the different GRBs correlations known insofar assuming a fiducial Λ CDM model in agreement with the recent WMAP5 data. Averaging over six correlations, we end with a new GRBs Hubble diagram comprising 83 objects. We also extensively explore the impact of varying the fiducial cosmological model considering how the estimated $\mu(z)$ change as a function of the (Ω_M, w_0, w_a) parameters of the Chevallier - Polarski - Linder phenomenological dark energy equation of state. In order to avoid the need of assuming an *a priori* cosmological model, we present a new calibration procedure based on a model independent local regression estimate of $\mu(z)$ using the Union SNeIa sample to calibrate the GRBs correlations. This finally gives us a GRBs Hubble diagram made out of 69 GRBs whose estimated distance modulus $\mu(z)$ is almost independent on the underlying cosmological model.

Key words: Gamma Rays: bursts – Cosmology: distance scale – Cosmology: cosmological parameters

1 INTRODUCTION

The Hubble diagram of Type Ia Supernovae (SNeIa) provided the first evidence of the cosmic speed up (Perlmutter et al. 1997; Riess et al. 1998) opening the way to a flood of theoretical and observational efforts devoted to investigate the nature and the nurture of such a phenomenon. The astrophysical data coming from later SNeIa samples (Riess et al. 2007; Astier et al. 2006; Wood-Vasey et al. 2007; ?; Davis et al. 2007; Kowalski et al. 2008), Baryonic Acoustic Oscillations (Eisenstein et al. 2005; Percival et al. 2007), the anisotropy spectrum of cosmic microwave background radiation (de Bernardis et al. 2000; Bennett et al. 2003; Bennett et al. 2003; Dunkley et al. 2008) and the large scale structure data from large galaxy redshift surveys (Dodelson et

al. 2002; Percival et al. 2002; Szalay et al. 2003; Hawkins et al. 2003) have strengthened the then surprising result. As a consequence, there is nowadays little doubt that the universe is spatially flat, has a low matter content ($\Omega_M \simeq 0.3$) and is undergoing a phase of accelerated expansion. To close the energy budget and drive the cosmic speed up, a new fluid with negative pressure dubbed dark energy has been invoked as the only viable solution. Understanding what dark energy really is stands out as one of the most fascinating problems of modern cosmology. Roughly speaking, we can divide the different proposals in two broad categories. In the first class, one can include all models considering dark energy as a true fluid with unusual properties with proposals ranging from the classical cosmological constant Λ (Carroll et al. 1992; Sahni & Starobinski 2000) to scalar fields running down their

self interaction potential (Peebles & Rathra 2003; Padmanabhan 2003; Copeland et al. 2006). On the other hand, one may give off General Relativity resorting to modified gravity theories such as $f(R)$ models (see, e.g., Capozziello et al. 2008, Sotiriou & Faraoni 2008 and references therein) and braneworld cosmologies (Dvali et al. 2000; Lue et al. 2004) manifesting themselves as a fictitious dark energy - like fluid.

Notwithstanding their radically different inspiring philosophies, all the viable theories share the same ability to be in satisfactory agreement with the available data. Such a confusing situation is a clear evidence that present dataset are unable to discriminate among different models. Such a problem comes out as a consequence of the still low redshift range probed. The SNeIa Hubble diagram is an illuminating example. As well known, the distance modulus $\mu(z)$ scales linearly with the logarithm of the luminosity distance $d_L(z)$ which depends on the dark energy equation of state through a double integration. Discriminating among different models asks for extending the Hubble diagram to higher redshifts since the expressions for the $H(z)$ and hence $\mu(z)$ are more and more different as one goes to higher and higher z values.

Unfortunately, such a project can not be undertaken relying on SNeIa since, even with excellent space based projects such as SNAP (Aldering et al. 2004), it is almost impossible going to $z > 2$. Indeed, up to now, most of the SNeIa observed have redshift $z \leq 1.2$ with only one SN at $z = 1.7$. On the contrary, Gamma Ray Bursts (GRBs) are ideal candidates from this point of view. Indeed, thanks to their enormous energy release, they have been observed up to redshift $z > 5$, the most distant one being GRB080913 with $z = 6.7$ (Greiner et al. 2008). as high as $z \simeq 6.5$. There is, however, a fierce problem to overcome. Actually, GRBs are not standard candles so that it is not immediately possible to build their Hubble diagram. To this aim, one has to look for a correlation between a distance dependent quantity and a directly observable property. Many of these correlations have been suggested in the last few years so that the route towards making GRBs standardizable candles (in the same way as SNeIa) is now open.

Actually, various attempts to build a GRBs Hubble diagram have yet been made. Bradley (2003) first derived the luminosity distances of 9 GRBs with known redshifts by using two GRBs luminosity relations thus providing the first GRBs Hubble diagram. Dai et al. (2004) and Xu et al. (2005) have then proposed a methodology to constrain cosmological parameters using GRBs and apply it to preliminary samples (made out of 12 and 17 objects respectively) relying on the Ghirlanda relation. A Bayesian based approach was instead proposed by Firmani et al. (2005), later improved by the same authors (Firmani et al. 2006) advocating the joint use of GRBs and SNeIa.

As a first summary of these efforts, Schaefer (2007) has compiled a catalog of 69 GRBs with measured properties entering the five two parameters correlation then available. Estimating $\mu(z)$ from each single correlation and performing a weighted average, Schaefer have finally built the first GRBs Hubble diagram which has later been used in different cosmological analyses (Wright 2007; Wang et al. 2007; Li et al. 2008; Daly et al. 2008; Capozziello & Izzo 2008). We update here the Schaefer work by many aspects. First, we add the recently found $L_X T_a$ correlation (Dainotti et al. 2008) with L_X the X-ray luminosity at the time T_a and T_a a timescale

characterizing the late afterglow decay. The use of this new correlation allows us to both increase the GRBs sample and reduce the uncertainty on $\mu(z)$. We then recalibrate all the six correlations considered using a fiducial Λ CDM cosmological model in agreement with the WMAP5 (Dunkley et al. 2008) data and a Bayesian motivated fitting technique (D'Agostini 2005). We are now able to build a new GRBs Hubble diagram whose dependence on the background cosmological model used for the calibration is explored. Finally, we present a novel method to escape the circularity problem, i.e. to calibrate the GRBs empirical laws without assuming any a priori cosmological model. This gives us then the possibility to build up a new GRBs Hubble diagram less affected by systematic uncertainties related to the unknown cosmological scenario.

The plan of the paper is as follows. In Sect. 2, we briefly review the different GRBs 2D correlations known insofar and present the Bayesian motivated method we will use in the following to calibrate them. Such a calibration is performed in Sect. 3.1 using a fiducial Λ CDM model with parameters set according to the recent WMAP5 results. These calibrated relations are then used in Sect. 3.2 to build a Hubble diagram comprising 83 objects, while Sect. 3.3 explores what is the impact of varying the cosmological model used in the calibration on the estimated distance modulus. Sect. 4.1 presents the local regression method showing how it is possible to use the Union SNeIa sample to recover the value of $\mu(z)$ in a cosmological model independent way. This method is then used to calibrate the 2D correlations for the GRBs with $z \leq 1.4$ in Sect. 4.2 so that a newly calibrated GRBs Hubble diagram may be built in Sect. 4.3 where we also compare this latter to the fiducial one. The impact of different kind of systematics on the derived Hubble diagrams is investigated in Sect. 5. Having thus checked the reliability of the GRBs HDs thus obtained, we present in Sect. 6 a first cosmological analysis and discusses the importance of GRBs as a cosmological tool presenting a forecast of the precision affordable on the matter density parameter, Ω_M , and the dark energy equation of state. Finally, Sect. 7 is devoted to the conclusions, while in the Appendix we tabulate the estimated distance modulus from the two different methods and make some few comments on possible outliers.

2 TWO PARAMETERS CORRELATIONS

In order to be as general as possible, let us denote with x a distance independent property and let $y = kd_L^2(z)$ a given quantity with k a redshift independent constant and $d_L(z)$ the luminosity distance. Let us suppose that we have been able to find a correlation between them such as:

$$\log y = k + 2 \log d_L(z) = a + b \log x .$$

Should the relation be calibrated, i.e. the parameters (a, b) be known, we can then use it to compute the distance modulus $\mu(z)$ of an object at redshift z simply as:

$$\begin{aligned} \mu(z) &= 25 + 5 \log d_L(z) \\ &= 25 + (5/2)(\log y - k) \\ &= 25 + (5/2)(a + b \log x - k) \end{aligned}$$

where all the quantities are now known.

Notwithstanding its conceptual simplicity, performing such a program for GRBs is far to be trivial. First, one has to find such a two parameters (hereafter, 2D) correlation, i.e. decide what are the quantities (x, y) . As we will see, there are different choices which seems to work satisfactorily well, but the intrinsic scatter around the best fit line is usually not negligible. Moreover, it is still not clear what is the underlying physical mechanism originating the empirical 2D correlations found. As a second more important problem, calibrating such relations is a still open problem. Indeed, since local GRBs, i.e. GRBs with $z < 0.01$, are not available, the only one being GRB 980425 (Galama et al. 1998), one has typically assume an a priori cosmological model to compute $d_L(z)$ and hence y so that the calibration turns out to be model dependent thus leading to the well known circularity problem when one aims at using GRBs as cosmological probes. As a third problem, the calibration procedure is performed using a variety of statistical methods so that the results from the use of different correlations can not be straightforwardly compared.

In the following, we first briefly review the known 2D correlations and then describe a Bayesian motivated fitting procedure to determine the calibration parameters (a, b) and the intrinsic scatter σ_{int} once a GRB sample is available.

2.1 2D empirical laws

The 2D correlations we will discuss here typically relate a GRB observable with the isotropic absolute luminosity L or the collimation corrected energy E_γ , with a single case correlating with the X-ray afterglow luminosity. On the other hand, the observable properties cover a wide range of GRBs features including both quantities related to the energy spectrum and the light curve. In the first class, we find the peak energy E_p , which is the energy at which the νF_ν spectrum is brightest, and the time lag τ_{lag} , which measures the time offset between the arrival of the low and high energy photons. To the light curve shape are instead related the rise time τ_{RT} , which is the shortest time over which the light curve rises by half the peak flux of the burst, and the variability V , which quantifies the smoothness of the light curve itself. Somewhat different is the $L_X - T_a$ correlation, with L_X the luminosity at the time T_a and T_a a time scale, both referring to the X-ray afterglow decay curve.

As yet said, neither L nor E_γ are directly measurable quantities since they depend on the luminosity distance $d_L(z)$. Indeed, it is :

$$L = 4\pi d_L^2(z) P_{bolo}, \quad (1)$$

$$E_\gamma = 4\pi d_L^2(z) S_{bolo} F_{beam} (1+z)^{-1}. \quad (2)$$

Here, P_{bolo} and S_{bolo} are the bolometric peak flux and fluence, respectively, while $F_{beam} = 1 - \cos \theta_{jet}$ is the beaming factor with θ_{jet} the rest frame time of achromatic break in the afterglow light curve. Note that P_{bolo} and S_{bolo} are computed from the observed GRB energy spectrum $\Phi(E)$ as follows (Schaefer 2007) :

$$P_{bolo} = P \times \frac{\int_{1/(1+z)}^{10^4/(1+z)} E\Phi(E)dE}{\int_{E_{min}}^{E_{max}} E\Phi(E)dE}, \quad (3)$$

$$S_{bolo} = S \times \frac{\int_{1/(1+z)}^{10^4/(1+z)} E\Phi(E)dE}{\int_{E_{min}}^{E_{max}} E\Phi(E)dE}, \quad (4)$$

with P and S the observed peak energy and fluence in units of erg/cm²/s and erg/cm², respectively, and (E_{min}, E_{max}) the detection thresholds of the observing instrument. Note that the energy spectrum is modelled using a smoothly broken power-law (Band et al. 1993) which reads :

$$\Phi(E) = \begin{cases} AE^\alpha e^{-(2+\alpha)E/E_p} & E \leq [(\alpha - \beta)/(2 + \alpha)]E_p \\ BE^\beta & \text{otherwise} \end{cases}. \quad (5)$$

While L and E_γ are bolometric quantities, we will also consider a recently found 2D correlations involving only X-ray observables. In particular, we will therefore be concerned with the luminosity in the X-ray. As a general rule, if we denote by $L_X(t)$ and $F_X(t)$ the luminosity and the flux at the time t in the afterglow light curve, one can write :

$$L_X(t) = 4\pi d_L^2(z) F_X(t) \quad (6)$$

where the flux must be K -corrected (Bloom et al. 2001) as :

$$F_X(t) = f(t) \times \frac{\int_{E_{min}/(1+z)}^{E_{max}/(1+z)} E\Phi_X(E)dE}{\int_{E_{min}}^{E_{max}} E\Phi_X(E)dE} \quad (7)$$

with $(E_{min}, E_{max}) = (0.3, 10)$ keV set by the instrument bandpass and $\Phi_X(E)$ the energy spectrum in the X-ray band, well approximated as a single power law. Finally, $f(t)$ describes the time variation of the flux along the afterglow curve and is parametrized as given in Willingale et al. (2007). Note that Eq.(6) is the same as Eq.(1) the only difference being the integration limits at the numerator. Actually, while L is the bolometric luminosity, L_X refers to the X-ray one so that we integrate only over this energy range.

As an important remark, it is worth stressing that all the 2D correlations we will use refer to quantities evaluated in the GRB rest frame, while the observed spectra and light curves are in the Earth orbiting satellite frames. As such, they are affected by time dilation and redshifting which have to be corrected for before the calibration procedure. All of the 2D correlations available insofar are power-laws so that it is useful to work in logarithmic units. As a general rule, we will therefore consider a linear rule as :

$$\log R = a \log Q + b \quad (8)$$

where R is a distance dependent quantity, while Q is not. Different choices for (R, Q) determine the different 2D empirical laws. Setting $R = E_\gamma$ and $Q = E_p(1+z)/300$ keV (where the factor $(1+z)$ corrects for redshifting) gives the Ghirlanda relation (Ghirlanda et al. 2004; Ghirlanda et al. 2006). It is worth noting that this is the only relation involving an energy quantity, the other ones always involving a luminosity as R quantity. Indeed, setting $R = L$, we can find 2D correlations for $Q = E_p(1+z)/300$ keV (Schaefer 2003; Yonekoku et al. 2004), $Q = \tau_{lag}(1+z)^{-1}/0.1$ s (Norris et al. 2000), $Q = \tau_{RT}(1+z)^{-1}/0.1$ s (Schaefer 2007) and $Q = V(1+z)/0.02$ (Fenimore & Ramirez-Ruiz 2000; Riechart et al. 2001; Schaefer 2007). Note that in all these correlations the factor $(1+z)$ or $(1+z)^{-1}$ corrects for time dilation or redshifting, while the normalization is chosen in

order to minimize the correlation between the errors. Finally, setting $R = L_X(T_a)$ and $Q = T_a/(1+z)$ gives the 2D correlation empirically found for the first time in Dainotti et al. (2008) and later confirmed by Ghisellini et al. (2008) on a semitheoretical basis and by Yamazaki (2008) in the framework of his model proposed to explain the observed plateau in the X-ray GRBs afterglows.

2.2 Bayesian fitting procedure

Eq.(8) is a linear relation which can be fitted to a given dataset (Q_i, R_i) in order to determine the two calibration parameters (a, b) . Actually, the situation is not so simple as one may naively expect. Indeed, both the (Q, R) variables are affected by measurement uncertainties (σ_Q, σ_R) which can not be neglected. Moreover, $\sigma_Q/Q \sim \sigma_R/R$ so that the simple rule to choose as independent variable in the fit the one with the smallest relative error can not be applied here. Finally, the 2D correlations we are interested in are still not definitively explained by an underlying theoretical model determining the detailed features of the GRBs explosion and afterglow phenomenology. Both on theoretical and observational grounds, we do expect a certain amount of intrinsic scatter around the best fit line which has to be taken into account and determine together with (a, b) by the fitting procedure. Different statistical recipes are available to cope with these problems with each author having its own preferences. How the fitting technique employed affects the final estimate of the distance modulus for a given GRB from the different 2D correlations is not clear so that it is highly desirable to recalibrate all of them with the same method.

To this aim, in the following we will resort to a Bayesian motivated technique (D' Agostini 2005) thus maximizing the likelihood function $\mathcal{L}(a, b, \sigma_{int}) = \exp[-L(a, b, \sigma_{int})]$ with :

$$L(a, b, \sigma_{int}) = \frac{1}{2} \sum \ln(\sigma_{int}^2 + \sigma_{R_i}^2 + a^2 \sigma_{Q_i}^2) + \frac{1}{2} \sum \frac{(R_i - aQ_i - b)^2}{\sigma_{int}^2 + \sigma_{R_i}^2 + a^2 \sigma_{Q_i}^2} \quad (9)$$

where the sum is over the \mathcal{N} objects in the sample. Note that, actually, this maximization is performed in the two parameter space (a, σ_{int}) since b may be estimated analytically as :

$$b = \left[\sum \frac{R_i - aQ_i}{\sigma_{int}^2 + \sigma_{R_i}^2 + a^2 \sigma_{Q_i}^2} \right] \left[\sum \frac{1}{\sigma_{int}^2 + \sigma_{R_i}^2 + a^2 \sigma_{Q_i}^2} \right]^{-1} \quad (10)$$

so that we will not consider it anymore as a fit parameter.

It is worth noting that the Bayesian approach allows to find out what is the most likely set of parameters within a given theory, but does not tell us whether this model fits well or not the data. An easy way to quantitatively estimate the goodness of the fit is obtained considering the median and root mean square of the best fit residuals, defined as $\delta = R_{obs} - R_{fit}$ which we will also compute for the different 2D correlations we will consider.

The Bayesian approach used here also allows us to quantify the uncertainties on the fit parameters. To this aim, for a given parameter p_i , we first compute the marginalized likelihood $\mathcal{L}_i(p_i)$ by integrating over the other parameter. The median value for the parameter p_i is then found by solving :

$$\int_{p_{i,min}}^{p_{i,med}} \mathcal{L}_i(p_i) dp_i = \frac{1}{2} \int_{p_{i,min}}^{p_{i,max}} \mathcal{L}_i(p_i) dp_i . \quad (11)$$

The 68% (95%) confidence range $(p_{i,l}, p_{i,h})$ are then found by solving :

$$\int_{p_{i,l}}^{p_{i,med}} \mathcal{L}_i(p_i) dp_i = \frac{1-\varepsilon}{2} \int_{p_{i,min}}^{p_{i,max}} \mathcal{L}_i(p_i) dp_i , \quad (12)$$

$$\int_{p_{i,med}}^{p_{i,h}} \mathcal{L}_i(p_i) dp_i = \frac{1-\varepsilon}{2} \int_{p_{i,min}}^{p_{i,max}} \mathcal{L}_i(p_i) dp_i , \quad (13)$$

with $\varepsilon = 0.68$ (0.95) for the 68% (95%) range respectively.

3 UPDATING THE GRB HUBBLE DIAGRAM

Following the classical approach, we calibrate the six 2D correlations described above by first estimating the distance dependent quantity (namely, E_γ , L or L_X) in a given cosmological model. In particular, to be in agreement with the most recent results, we choose a fiducial spatially flat concordance Λ CDM model with $\Omega_M = 1 - \Omega_\Lambda = 0.291$ and $h = 0.697$ as suggested by the analysis of the WMAP5 data (Dunkley et al. 2008). The sample of GRBs used is the one compiled by Schaefer (2007) for the first five 2D correlations, while the $L_X - T_a$ law is calibrated using a subsample of the Willingale et al. (2007) catalog made out of 28 GRBs with measured redshift, $\log L_X(T_a) \geq 45$ and $1 \leq \log [T_a/(1+z)] \leq 5$ (see Dainotti et al. 2008 for the motivation of these cuts).

3.1 The calibration parameters

The Bayesian fitting procedure described above then gives us the results summarized in Table 1. It is worth stressing that, since the calibration parameters have been obtained using the same statistical analysis for all the 2D correlations, it is now possible to compare the relations avoiding any possible bias introduced by the different fitting procedure.

As a first issue, one can qualitatively judge what is the best correlation, i.e. what is the correlation giving the smaller residuals or having the smaller intrinsic scatter. From an observational point of view, there is not a 2D law working significantly better than the other ones since both δ_{med} and δ_{rms} take almost the same values over the full set, with only a modest preference for the $E_\gamma - E_p$, $L - \tau_{lag}$ and $L_X - T_a$ correlations. On a theoretical side, one can argue that the 2D law having the smallest intrinsic scatter is the better motivated one since the (unknown) underlying physical mechanism works in the same way for all the GRBs involved. Taken at face values, the maximum likelihood estimates for σ_{int} should argue in favour of the $E_\gamma - E_p$ and $L_X - T_a$ correlations, but this conclusion becomes meaningless when one takes into account the 68% and 95% confidence ranges which overlap quite well.

Finally, we caution the reader that we have implicitly assumed that the calibration parameter do not change with the redshift notwithstanding the fact that z spans a quite large range (from $z = 0.125$ up to $z = 6.6$). The limited number of GRBs makes it not possible to explore in detail the validity of this usually adopted working hypothesis, but we can get a hint by considering whether the residuals correlate with the redshift. The values reported in Table 1

Table 1. Calibration parameters (a, b) and intrinsic scatter σ_{int} for the 2D correlations $\log R = a \log Q + b$ in a fiducial Λ CDM model. Columns are as follows: 1. id of the correlation with the first letter referring to the R variable and the second to the Q quantity; 2. number of GRBs used; 3. maximum likelihood parameters; 4, 5, 6. median, root mean square and Spearman rank correlation parameter with the redshift of the best fit residuals; 7, 8. median value and 68 and 95% confidence ranges for the parameters (a, σ_{int}) .

Id	\mathcal{N}	$(a, b, \sigma_{int})_{ML}$	δ_{med}	δ_{rms}	$C(\delta, z)$	$a_{-1\sigma}^{+1\sigma} \quad +2\sigma \quad -2\sigma$	$(\sigma_{int})_{-1\sigma}^{+1\sigma} \quad +2\sigma \quad -2\sigma$
$E_\gamma - E_p$	27	(1.38, 50.56, 0.25)	0.01	0.38	-0.17	$1.37_{-0.26}^{+0.23} \quad +0.48 \quad -0.30$	$0.30_{-0.09}^{+0.11} \quad +0.28 \quad -0.16$
$L - E_p$	64	(1.24, 52.16, 0.45)	-0.05	0.51	0.07	$1.24_{-0.18}^{+0.18} \quad +0.36 \quad -0.36$	$0.48_{-0.07}^{+0.07} \quad +0.17 \quad -0.12$
$L - \tau_{lag}$	38	(-0.80, 52.28, 0.37)	0.02	0.40	0.40	$-0.80_{-0.14}^{+0.14} \quad +0.30 \quad -0.30$	$0.40_{-0.07}^{+0.09} \quad +0.21 \quad -0.12$
$L - \tau_{RT}$	62	(-0.89, 52.48, 0.44)	0.04	0.47	0.27	$-0.89_{-0.18}^{+0.16} \quad +0.31 \quad -0.38$	$0.46_{-0.06}^{+0.07} \quad +0.16 \quad -0.11$
$L - V$	51	(1.03, 52.49, 0.48)	-0.09	0.50	0.25	$1.04_{-0.29}^{+0.39} \quad +0.60 \quad -0.57$	$0.51_{-0.07}^{+0.09} \quad +0.21 \quad -0.13$
$L_X - T_a$	28	(-0.58, 48.09, 0.33)	-0.12	0.43	-0.21	$-0.58_{-0.18}^{+0.18} \quad +0.38 \quad -0.37$	$0.39_{-0.11}^{+0.14} \quad +0.33 \quad -0.20$

shows that only a weak and not significant correlation exists thus arguing in favour of the starting hypothesis. This is in agreement with what has recently been found by Basilikos & Perivolaropoulos (2008) which have calibrated the first five 2D correlations in Table 1 dividing the GRBs in redshift bins. Although they used a different fitting technique so that our results can not be directly compared to their ones, we nonetheless agree with their conclusion that no statistical evidence of a dependence of the (a, b, σ_{int}) parameters on the redshift is present.

3.2 Making up the GRBs Hubble diagram

Once the six 2D correlations have been calibrated, we can now use them to compute the GRBs Hubble diagram. In order to reduce the error and, in a sense, marginalize over the possible systematic biases present in each one of the correlations, we follow Schaefer (2007) and take a weighted average of the distance modulus provided by each one of the six 2D laws in Table 1. As a preliminary step, let us remember that the luminosity distance of a GRB with redshift z may be computed as:

$$d_L(z) = \begin{cases} E_\gamma(1+z)/4\pi F_{beam} S_{bolo} \\ L/4\pi P_{bolo} \\ L_X(1+z)^{\beta_a+2}/4\pi F_X(T_a) \end{cases} \quad (14)$$

depending on whether a correlation involving E_γ , L or L_X is used*. The uncertainty on $d_L(z)$ is then estimated through the naive propagation of the measurement errors on the involved quantities. In particular, the error on the distance dependent quantity R is estimated as:

$$\sigma(\log R) = \sqrt{a^2 \sigma^2(\log Q) + \sigma_{int}^2} \quad (15)$$

* Note that the factor $(1+z)^{\beta_a+2}$ in the formula involving L_X come from the k-correction of the flux $F_X(T_a)$ with β_a being the slope of the power-law energy spectrum in the X-ray band.

and is then added in quadrature to the other terms entering Eq.(14) to get the total uncertainty. The distance modulus $\mu(z)$ is easily obtained from its definition:

$$\mu(z) = 25 + 5 \log d_L(z) \quad (16)$$

with its uncertainty obtained again by error propagation. Following Schaefer (2007), we finally estimate the distance modulus for the i -th GRB in the sample at redshift z_i as:

$$\mu(z_i) = \left[\sum_j \mu_j(z_i)/\sigma_{\mu_j}^2 \right] \times \left[\sum_j 1/\sigma_{\mu_j}^2 \right]^{-1} \quad (17)$$

with the uncertainty given by:

$$\sigma_\mu = \left[\sum_j 1/\sigma_{\mu_j}^2 \right]^{-1} \quad (18)$$

where the sum runs over the 2D empirical laws which can be used for the GRB considered. Joining the Willingale et al. (2007) and Schaefer (2007) samples and considering that 17 objects are in common, we end up with a catalogo of 83 GRBs which we use to build the Hubble diagram plotted in Fig.1 and tabulated in the Appendix[†]. We will refer in the following to this dataset as the *fiducial* GRBs Hubble diagram (hereafter, HD) since it relies on a calibration made using a fiducial Λ CDM model to compute the distances.

It is worth comparing our fiducial HD to the one derived by Schaefer (2007) which we will refer to as the Schaefer HD. Actually, we have improved over the Schaefer HD by three aspects, namely updating the Λ CDM model parameters, using a Bayesian motivated fitting procedure and adding a further 2D correlation. To investigate the impact of these differences, we first consider the 69 Schaefer GRBs and compute the distance modulus with our new calibration,

[†] ASCII tables with the Hubble diagram and all the other datasets necessary to repeat the full analysis presented in this paper together with the *Mathematica* codes used are available on request to V.F. Cardone (winnynodrac@gmail.com).

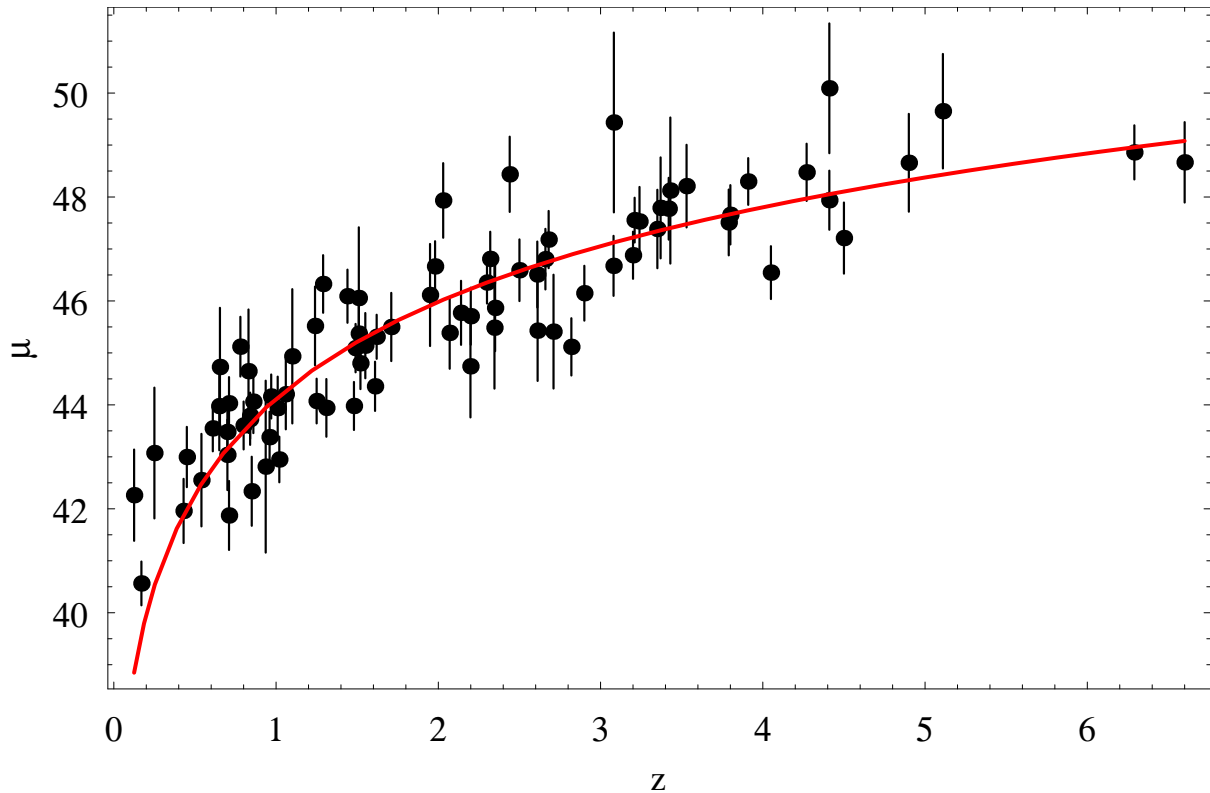


Figure 1. The fiducial GRBs Hubble diagram with overplotted the distance modulus predicted by the fiducial Λ CDM model.

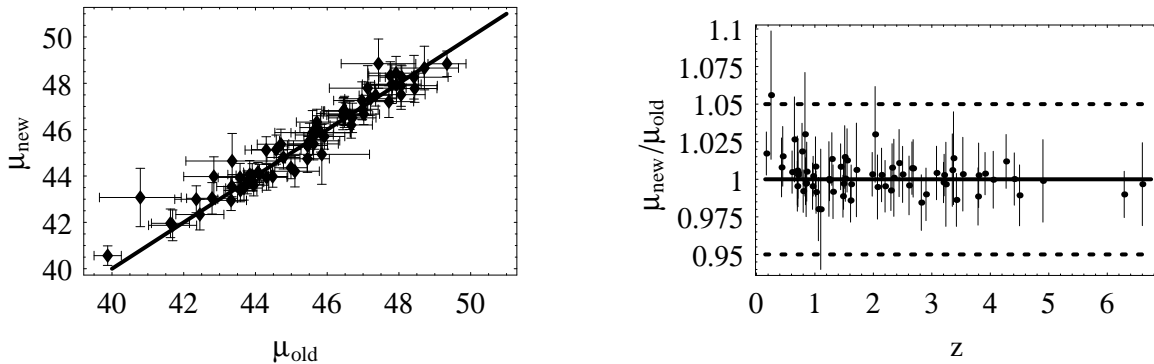


Figure 2. Comparison between $\mu(z)$ for the 69 Schaefer GRBs as computed by Schaefer and by us (denoted as μ_{old} and μ_{new} respectively).

but not including the values coming from the $L_X - T_a$ correlation. We then plot the in left panel of Fig. 2 the old vs the new estimates of the distance modulus. As can be seen, there is a clear one-to-one correspondence with slope perfectly compatible with 1 and no systematic offset. This can also be better appreciated looking at the right panel showing that μ_{new}/μ_{old} is close to 1 within the 5% with no correlation with the redshift. To be more quantitative, averaging over the 69 GRBs, we find $\mu_{new}/\mu_{old} = 1.00 \pm 0.01$ with an root mean square value $(\mu_{new}/\mu_{old})_{rms} = 1.002$. We may therefore safely conclude that the new calibration procedure have not affected the results.

A cautionary remark on the errors is in order here. As explained above, the uncertainty on μ comes from the propagation of the errors starting from the ones on the distance

dependent quantities E_γ , L or L_X . Comparing Eq.(15) with the similar formulae in Schaefer (2007), one can see that we have not included in the propagation the errors on the calibration coefficient (a, b). This is a direct consequence of the different statistical philosophy underlying the fitting procedure employed (Bayesian maximum likelihood here vs the frequentist χ^2 minimization in Schaefer). We have however checked whether this bias somewhat the error estimates. Averaging over the 69 GRBs, we find $\sigma_{new}/\sigma_{old} = 1.01 \pm 0.06$ with a root mean square value $(\sigma_{new}/\sigma_{old})_{rms} = 1.01$ and no correlation with the redshift. These numbers make us then confident that no under or overestimation of the errors is introduced by our different approach.

Having added the new $L_X - T_a$ correlation makes it possible to infer the distance modulus for further 14 objects thus

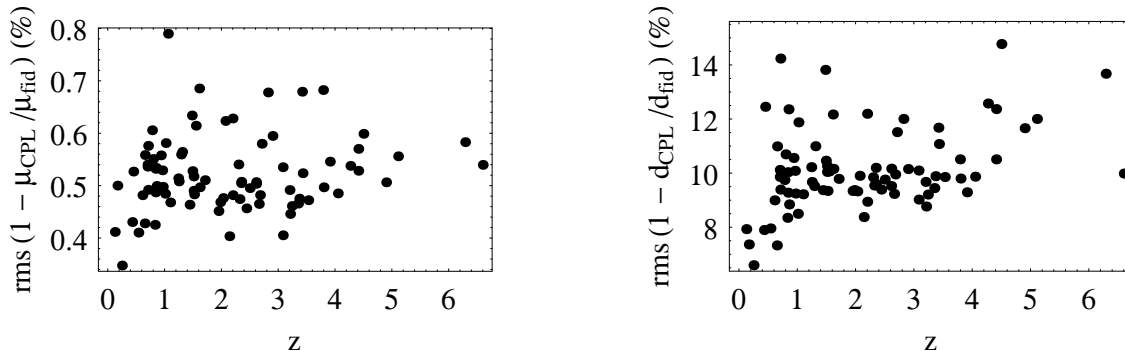


Figure 3. Root mean square of the percentage deviation of the distance modulus $\mu(z)$ (left) and the luminosity distance $d_L(z)$ from the fiducial Λ CDM values caused by changing the (w_0, w_a) parameters for $\Omega_M = 0.30$. Similar results are obtained for other Ω_M values.

leading to 83 the number of GRBs in the fiducial HD, i.e. 20% more data. Moreover, this also makes it possible to reduce the error thanks to the weighted averaging procedure employed. Indeed, in the old Schaefer HD, the numbers of GRBs with $\mu(z)$ estimated from 1 to 5 correlations are respectively (3, 12, 14, 27, 13). On the contrary, these numbers now read (17, 7, 16, 24, 16, 3) with 3 GRBs having μ computed from all the six 2D correlations. We do expect that this lead to a decrease of the uncertainty on $\mu(z)$. Averaging over the 83 objects, we indeed find $\sigma_\mu/\sigma_{Sch} = 0.86 \pm 0.09$ with $(\sigma_\mu/\sigma_{Sch})_{rms} = 0.87$, i.e. there is on average a significative 14% reduction.

Summarizing, the detailed analysis performed make us confident that the fiducial GRB HD plotted in Fig. 1 and tabulated in the Appendix represents a noteworthy step forward for using GRBs as cosmological tools.

3.3 Varying the cosmological model

The fiducial HD has been obtained after calibrating the six 2D correlations in Table 1 assuming a Λ CDM concordance cosmology. Although this model is in agreement with most of the available astrophysical data, there is still not a clear consensus on the value of its parameters (Ω_M, h) . Moreover, although not preferred by the data, a varying equation of state (EoS) for the dark energy fluid is still a viable (and theoretically better motivated) option. A large class of dark energy models predict a dependence of the EoS on the scale factor a which is well fitted by the Chevallier - Polarski - Linder (CPL) ansatz (Chevallier & Polarski 2001; Linder 2003):

$$w(a) = w_0 + w_a(1 - a) = w_0 + w_a z / (1 + z). \quad (19)$$

The luminosity distance is then computed as:

$$d_L(z) = \frac{c}{H_0} (1+z) \int_0^z \frac{dz'}{E(z')} \quad (20)$$

with $E(z) = H(z)/H_0$ given by:

$$E^2(z) = \Omega_M (1+z)^3 + \Omega_X (1+z)^{3(1+w_0+w_a)} e^{-\frac{3w_a z}{1+z}} \quad (21)$$

where $\Omega_X = 1 - \Omega_M$ because of the flatness assumption.

In order to quantify the impact of varying the EoS parameters (w_0, w_a) and the matter density Ω_M , we have recalibrated all the six 2D correlations on a regular grid in (w_0, w_a) for five different values of Ω_M . Namely, we consider

CPL models with $-1.3 \leq w_0 \leq -0.3$ and $-1.0 \leq w_a \leq 1.0$ for Ω_M from 0.20 to 0.40 in steps of 0.05. These ranges are larger than what is allowed by the data, but have been chosen in order to take into account also models very different from the fiducial one. For each point in the grid, we repeat all the steps described in the previous subsection to get the distance modulus to each GRB in the sample. We then collect these values and evaluate, for each GRB, the root mean square of the percentage deviation from the fiducial μ value. The results are plotted in the left panel of Fig. 3. Note that in this way we are performing a sort of average of the absolute percentage deviation so that, for instance, we can say that the distance modulus to a given GRB varies of order the number in the plot when (w_0, w_a) span the range considered above. Although averaging over different models is not motivated, we have checked that this simple procedure gives us the correct order of magnitude of the effect of changing the EoS and the matter content on the final Hubble diagram.

Looking at the left panel of Fig. 3, it is clear that the uncertainty on the background cosmological model to use in the calibration procedure is quite modest. Indeed, the distance modulus may be under or overestimated by a modest 0.5% with values never larger than 1%. This is the same order of magnitude and often smaller than the measurement uncertainty on $\mu(z)$ so that one can argue that our fiducial GRBs HD may be used even if the underlying cosmological model is different from the Λ CDM one we have assumed. Actually, this result is partly due to the use of the distance modulus rather than the luminosity distance directly. Indeed, as well known, a logarithmic scale always reduce the errors, an effect which is at work also in this case as can be understood looking at the right panel of Fig. 3. Here, we plot the same quantity as the left panel, but referring to the luminosity distance $d_L(z)$. The rms percentage deviation now increases to $\sim 10\%$ with values as large as 15% so that the impact of cosmology is more apparent. However, it is worth stressing that it is common practice to use the $\mu(z)$ rather than the $d_L(z)$ data when constraining cosmological models so that we can give off any further consideration of the reconstructed luminosity distance.

It is somewhat surprising that changing the cosmological model used for the calibration has such a small impact on the estimated $\mu(z)$. However, it is easy to trace back the origin of this unexpected result. Figs. 4 and 5 show the depen-

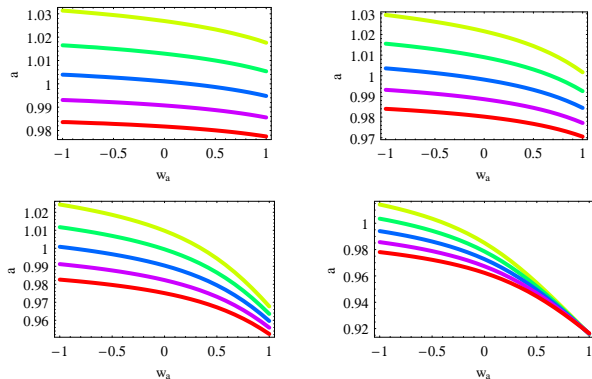


Figure 4. The dependence of the a coefficient of the $E_\gamma - E_p$ correlation normalized to the fiducial value on the w_a parameter for different values of w_0 (namely, $w_0 = -1.3, -1.0, -0.7, -0.4$ from top left to bottom right) and Ω_M (from 0.20 to 0.40 in steps of 0.05 from yellow higher to red lower curve).

dence on the (Ω_M, w_0, w_a) parameters of the slope coefficient a and the intrinsic scatter σ_{int} (normalized to their fiducial values) of the $E_\gamma - E_p$ correlation. Although there are clear trends, both a and σ_{int} change of order few % for the cosmological parameters spanning their quite conservative ranges. This is also the case for the other 2D correlations we have used so that we can deem this as a general result. This result then suggests that the calibration is in practice model independent, at least within the precision allowed by the present measurement uncertainties. As a consequence, the final Hubble diagram is almost unaffected by the choice of the cosmological model provided this can be well described within the framework of the CPL parameterization.

4 LOCAL REGRESSION CALIBRATION

Although the above analysis has shown that the choice of the underlying cosmological model has only a modest impact on the final estimate of the distance modulus, it is worth stressing that such a result is far to be definitive. First, we have considered only a single (although large) class of dark energy models. Moreover, one can argue that future data will be affected by smaller measurement uncertainties so that the impact of cosmology may turn out to be more important. It is therefore of vital importance to look for a method to calibrate the 2D correlations through a method that do not rely on the assumption of any cosmological model.

Due to the lack of a set of low redshift GRBs at $z < 0.1$ which are cosmology independent, the so called *circularity problem* arise: in order to use the GRBs as cosmological tools, one has to calibrate the 2D correlations, but a cosmological model has to be assumed for the calibration. In principle, such a problem could be avoided in two ways. First, a solid theoretical model must be found in order to physically motivate the observed 2D correlations thus setting their calibration parameters. Unfortunately, finding such a model remains an ambitious, but still unsuccessful task. Alternatively, it has been proposed to avoid the need for any distance determination by using a sufficiently large sample of GRBs within a small redshift bin centred at a whatever z (Ghirlanda et al. 2006; Liang & Zhang 2006). However,

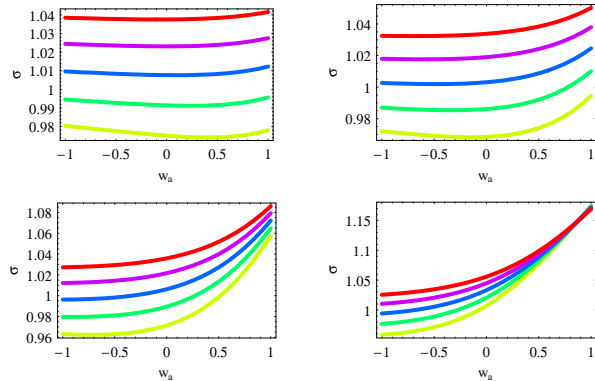


Figure 5. Same as Fig. 4, but for the intrinsic scatter σ_{int} . Note that Ω_M takes the same values as before, but now increases from the yellow lower to the red higher curve in each panel.

this method might be unrealistic, since the current sample of observed GRBs is not large enough. It has recently been suggested that such a model independent calibrations may be carried out using SNeIa as distance indicator based on the naive observations that a GRBs at redshift z must have the same distance modulus of SNeIa having the same redshift. Interpolating therefore the SNeIa Hubble diagram gives therefore the value of $\mu(z)$ for a subset of the GRBs sample with $z \leq 1.4$ which can then be used to calibrate the 2D correlations (Kodama et al. 2008; Liang et al. 2008; Wei & Zhang 2008). Assuming that this calibration is redshift independent, one can then build up the Hubble diagram at higher redshifts using the calibrated correlations for the remaining GRBs in the sample. We present here a similar approach still using the SNeIa as secondary distance indicator, but avoiding the need for interpolating the sparse dataset through the use of the local regression method we briefly describe in the following.

4.1 Local regression on SNeIa

As a general rule, any interpolation procedure may be seen as an attempt of recovering the true underlying curve from a sparse dataset. In a sense, interpolating methods try to extract the order of a smooth model from the disorder of the data originating from that same model. Interpolation may therefore be seen as a smoothing procedure so that one can naturally resort to the well tested strategies developed in this field. A particularly efficient method is known as *local regression* (see Loader 1999 and references therein).

Originally proposed by Cleveland (1979) and further developed by Cleveland and Devlin (1988), the local regression technique combines much of the simplicity of linear least squares regression with the flexibility of nonlinear regression. The basic idea relies on fitting simple models to localized subsets of the data to build up a function that describes the deterministic part of the variation in the data, point by point. Actually, one is not required to specify a global function of any form to fit a model to the data so that there is no ambiguity in the choice of the interpolating function. Indeed, at each point, a low degree polynomial is fit to a subset of the data containing only those points which are nearest to the point whose response is being estimated. The

Table 2. Calibration parameters (a, b) and intrinsic scatter σ_{int} for the 2D correlations $\log R = a \log Q + b$ for GRBs with $z \leq 1.4$ and distance modulus estimated from the local regression on SNeIa. Columns as in Table 1.

Id	\mathcal{N}	$(a, b, \sigma_{int})_{ML}$	δ_{med}	δ_{rms}	$\mathcal{C}(\delta, z)$	$a_{-1\sigma}^{+1\sigma} {}_{-2\sigma}^{+2\sigma}$	$(\sigma_{int})_{-1\sigma}^{+1\sigma} {}_{-2\sigma}^{+2\sigma}$
$E_\gamma - E_p$	12	(1.53, 50.59, 0.12)	0.10	0.22	0.22	$1.54_{-0.27}^{+0.30} {}_{-0.66}^{+0.74}$	$0.19_{-0.11}^{+0.17} {}_{-0.17}^{+0.43}$
$L - E_p$	25	(1.40, 52.20, 0.40)	0.06	0.45	0.12	$1.40_{-0.24}^{+0.25} {}_{-0.51}^{+0.53}$	$0.46_{-0.10}^{+0.14} {}_{-0.18}^{+0.34}$
$L - \tau_{lag}$	13	(-0.89, 52.07, 0.32)	0.11	0.35	0.33	$-0.90_{-0.27}^{+0.27} {}_{-0.64}^{+0.61}$	$0.42_{-0.13}^{+0.23} {}_{-0.22}^{+0.61}$
$L - \tau_{RT}$	24	(-0.97, 52.40, 0.44)	0.04	0.47	0.33	$-0.97_{-0.27}^{+0.27} {}_{-0.57}^{+0.57}$	$0.50_{-0.11}^{+0.15} {}_{-0.18}^{+0.36}$
$L - V$	19	(1.14, 52.33, 0.54)	-0.04	0.56	0.24	$1.19_{-0.61}^{+0.67} {}_{-1.39}^{+1.47}$	$0.64_{-0.15}^{+0.22} {}_{-0.25}^{+0.57}$

polynomial is fit using weighted least squares with a weight function which quickly decreases with the distance from the point where the model has to be recovered.

We apply local regression to estimate the distance modulus $\mu(z)$ from the most updated SNeIa sample. Referred to as Union (Kowalski et al. 2008), this compilation includes recent large samples from SNLS (Astier et al. 2006) and ESSENCE (Wood-Vasey et al. 2007) surveys, older data sets and the recently extended data set of distant SNeIa observed with HST, all of which have been homogenously re-analyzed with the same lightcurve fitter. After selection cuts and outliers removal, the final sample contains 307 SNeIa spanning the range $0.015 \leq z \leq 1.55$. We use this large dataset as input to the local regression estimate of $\mu(z)$ following the steps schematically sketched below.

- (i) Set a redshift z where $\mu(z)$ have to be recovered.
- (ii) Order the SNeIa according to increasing value of $|z - z_i|$ and select the first $n = \alpha \mathcal{N}_{SNeIa}$ with α a user selected value and \mathcal{N}_{SNeIa} the total number of SNeIa.

(iii) Define the weight function :

$$W(u) = \begin{cases} (1 - |u|^3)^3 & |u| \leq 1 \\ 0 & |u| \geq 1 \end{cases} \quad (22)$$

where $u = |z - z_i|/\Delta$ and Δ the maximum value of the $|z - z_i|$ over the subset chosen before.

(iv) Fit a first order polynomial to the data selected at step (ii) weighting each SNeIa with the corresponding value of the function $W(u)$ and take the zeroth order term as best estimate of $\mu(z)$.

(v) Estimate the error on $\mu(z)$ as the root mean square of the weighted residuals with respect to the best fit zeroth order term.

It is worth stressing that both the choice of the weight function and the order of the fitting polynomial are somewhat arbitrary. Similarly, the value of α to be used must not be too small in order to make up a statistical valuable sample, but also not too large to prevent the use of a low order

polynomial. In order to find what is the better value for α and simultaneously check that our choices for the polynomial degree and weight function do not affect the reconstruction, we have performed an extensive set of simulations. To this aim, we use the CPL EoS and set the model parameters (Ω_M, w_0, w_a, h) randomly extracting from the conservative ranges $0.15 \leq \Omega_M \leq 0.45$, $-1.5 \leq w_0 \leq -0.5$, $-2.0 \leq w_a \leq 2.0$, $0.60 \leq h \leq 0.80$. For each redshift value in the Union sample, we extract $\mu(z_i)$ from a Gaussian distribution centred on the theoretically predicted value and with a standard deviation $\sigma = 0.15$, in agreement with the estimated intrinsic scatter of the SNeIa absolute magnitude. To this value, we then attach an error in such a way that the relative uncertainty is the same as the corresponding point in the Union sample thus ending up with a mock catalogue having the same redshift and error distribution of the actual one. This mock catalogue is used as input to the routine sketched above and finally the reconstructed $\mu(z)$ value for each point in the catalog are compared to the input one.

Defining the percentage deviation $\delta\mu/\mu = 1 - \mu_{lr}(z)/\mu_{CPL}(z)$ with μ_{lr} and μ_{CPL} the local regression estimate and the input CPL values respectively and averaging over 250 realizations, we find that the above routine with the choice $\alpha = 0.025$ gives $(\delta\mu/\mu)_{rms} \simeq 0.35\%$ with $|\delta\mu/\mu| \leq 1\%$ independent on the redshift z . Moreover, there is no correlation at all of $\delta\mu/\mu$ with any of the cosmological parameters. We therefore safely conclude that the local regression method allows to correctly recover the underlying distance modulus at a whatever redshift z from the Union SNeIa sample whichever is the background cosmological model.

4.2 Model independent calibration

Having found an efficient way of estimating the distance modulus at redshift z in a model independent way, we can now calibrate the GRBs 2D correlation using a different approach. First, we consider only GRBs with $z \leq 1.4$ in order to cover the same redshift range spanned by the SNeIa data. As an example, let us consider the $L - E_p$ correlation. For each GRBs with measured (z, P_{bolo}) , one can write :

$$\begin{aligned} \log L &= \log(4\pi P_{bolo}) + 2 \log d_L(z) \\ &= \log(4\pi P_{bolo}) + (2/5) [\mu_{lr}(z) - 25] , \end{aligned}$$

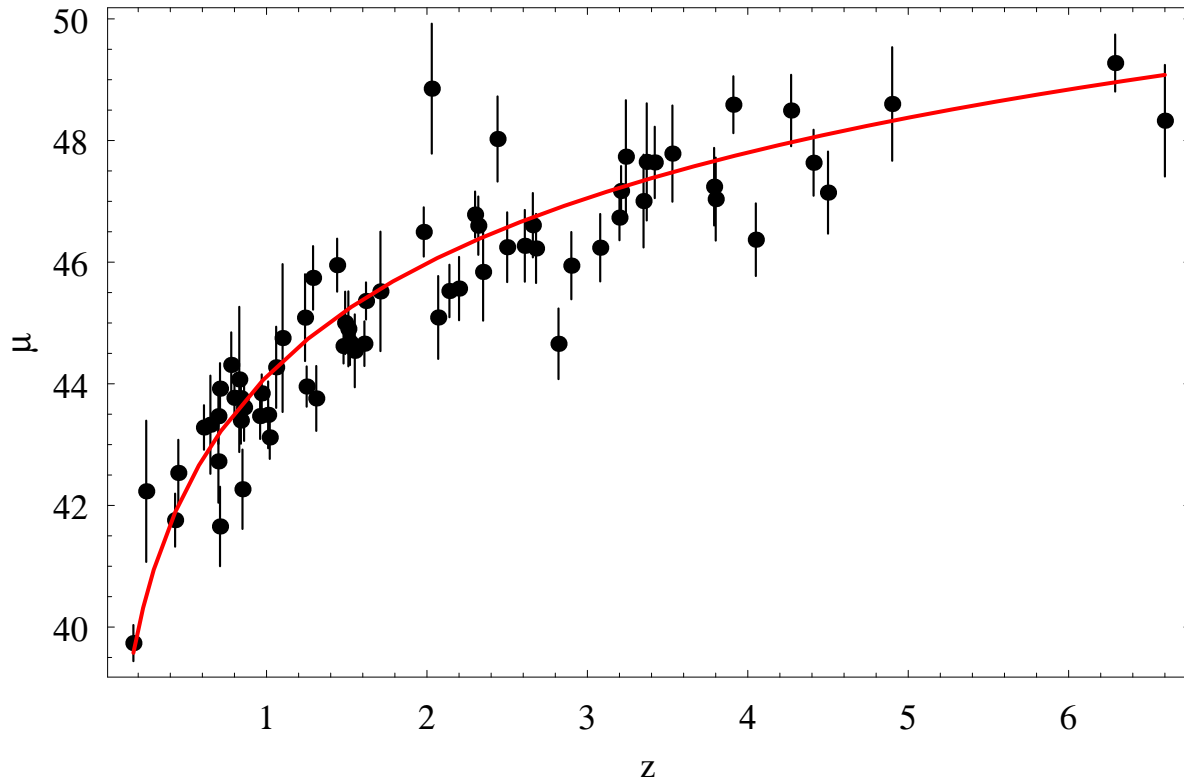


Figure 6. The calibrated Hubble diagram with overplotted the distance modulus predicted by the fiducial Λ CDM model.

where we have used Eq.(16) and approximated the true $\mu(z)$ with its local regression estimate $\mu_{lr}(z)$ without any significant loss of precision. The uncertainty on $\log L$ is then evaluated as usual by propagation of errors so that we finally end with a subset of GRBs with model independent estimates of $\log L$ that can be used as input to the Bayesian fitting procedure described in Sect. 2.2. Carrying on this exercise for the first five 2D correlations in Table 1, we get the results summarized in Table 2. Note that we cannot apply this method to the $L_X - T_a$ correlation since there are only 3 GRBs with $z \leq 1.4$ after the selection cuts on $\log [T_a/(1+z)]$ and $\log L_X$ so that the fitting fails.

Comparing the values in Tables 1 and 2, one should get some insight on the dependence of the calibration coefficients on the redshift. Taken at face values, it is apparent that fitting only $z \leq 1.4$ GRBs steepens all the 2D correlations, while the intrinsic scatter is almost unchanged in all cases but the $E_\gamma - E_p$ correlation. While this could naively be interpreted as an evidence for evolution with redshift of at least the slope, such a result loses its statistical significance when one looks at the marginalized constraints. Indeed, the 68 and 95% confidence ranges are quite larger than in the previous case so that inferring any constraints on the evolution of a is meaningless. Moreover, the present calibration is model independent, while the results in Table 1 have been obtained assuming a fiducial Λ CDM model. Although the discussion in Sect. 3.3 and Figs. 4 and 5 suggest that this should not be a serious problem, it is nevertheless worth being cautious before drawing any definitive conclusion.

4.3 The calibrated Hubble diagram

We can now use the calibration parameter derived above to infer the value of $\log R$ (with $R = E_\gamma$ or L) to construct a new GRBs Hubble diagram following the same method used in Sect. 3.2. The result is what we refer to as the *calibrated* GRBs HD. Plotted in Fig. 6 and tabulated in the Appendix, this HD now contains only the 69 Schaefer GRBs since we have not used the $L_X - T_a$ correlation being impossible to calibrate it with the local regression based method.

A visual comparison of Figs.1 and 6 shows that, although containing a different number of objects (83 vs 69), the fiducial and calibrated HDs are in well agreement. This is not unexpected since the fiducial Λ CDM model fits quite well the SNeIa data so that the predicted values for $\mu(z)$ are in very good agreement with the local regression estimates based on the same SNeIa. This qualitative agreement is also confirmed by considering the numbers of GRBs that are more than 2σ away from the theoretical fiducial Λ CDM HD. For the fiducial HD, we find 14 GRBs deviating more than 2σ , i.e. 17% of the sample, while this number reduces to 10, i.e. 14%, for the calibrated HD dataset. Moreover, the GRBs are almost the same[‡] thus arguing that there

[‡] The likely outliers GRBs for the fiducial dataset are: 990123, 991208, 991216, 000210, 010222, 020903, 030329, 030528, 050126, 050406, 060108, 060206, 060614. For the calibrated dataset, the list contains: 990123, 990506, 991208, 991216, 000210, 020813, 050406, 050603, 060108, 060206. There are thus 7 GRBs in common within the two lists. Note that 050603 is 3σ away in both datasets, while 060614 deviates more than 3σ from the fiducial

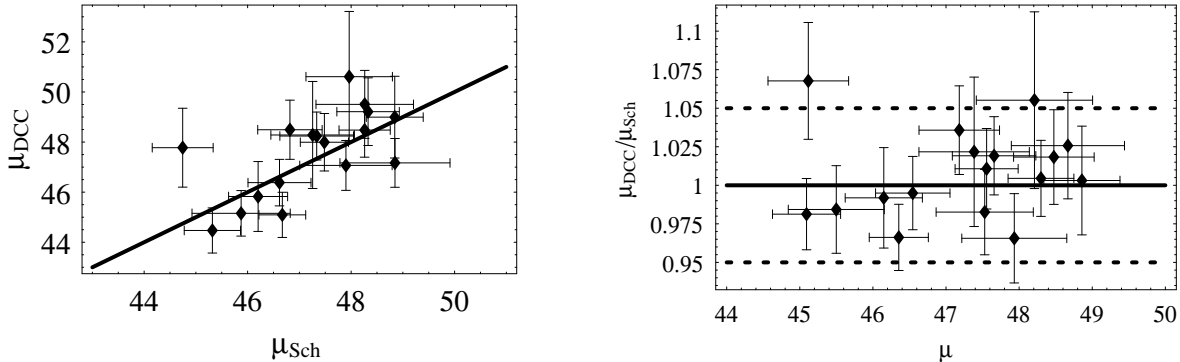


Figure 7. Comparison between $\mu(z)$ for the 17 GRBs common to the Schaefer and Willingale et al. samples.

is some problem with the data on this GRBs rather than with the procedure used to make up both the fiducial and the calibrated HDs. However, since we do not actually know whether the adopted fiducial Λ CDM model is indeed the correct one, we prefer to not reject these points in absence of a clear alternative motivation.

To quantitatively compare the fiducial and calibrated GRBs HDs, we have used a linear regression (not taking into account the errors on the two variables) to determine the slope of the $\mu_{fid} - \mu_{cal}$ relation, with μ_{fid} and μ_{cal} the distance modulus in the fiducial and calibrated HDs respectively. We find:

$$\mu_{fid} = (1.02 \pm 0.02)\mu_{cal} + (-1.28 \pm 0.94)$$

so that the slope is consistent with 1. It is worth stressing that the zeropoint of this relation does not signal a systematic offset, but is only a consequence of the slope being slightly different from 1. Indeed, defining $\Delta\mu = \mu_{fid} - \mu_{cal}$ and the averaging over the 69 GRBs in common, we find $\langle \Delta\mu \rangle = 0.20$ which is consistent with a null value if one takes into account the statistical errors on μ_{fid} and μ_{cal} .

Motivated by this successful comparison, we therefore conclude that the local regression based calibration has not biased anyway the derivation of the HD so that both the fiducial and the calibrated GRBs HDs can hence be used as valid tools to constrain cosmological models.

5 POSSIBLE SYSTEMATICS AND BIASES

While the previous analysis has shown that the calibrated and fiducial HDs are consistent with each other, such a test does not tell us nothing about possible systematic error related to the derivation of the underlying GRBs 2D correlations. Although a detailed analysis of the different systematic errors that can affect these relations is outside our aims here, we nevertheless investigate some related issues in order to qualitatively infer whether they can bias or not the derived distance moduli.

HD only. We also stress that only three GRBs (namely 050603, 060108, 060206) have $\mu(z)$ estimated also resorting to the $L_X - T_a$ correlation so that the use of this new empirical law can not be considered as a possible bias.

5.1 The $L_X - T_a$ correlation

The use of the $L_X - T_a$ correlation have allowed us to increase the GRBs sample from 69 to 83 objects[§]. However, since this is the first time such a correlation is used to build a GRBs HD, it is worth whether it is in agreement with the previous results. To this end, we have compared the estimated $\mu(z)$ for the 17 GRBs common to the Schaefer and Willingale et al. samples. This is shown in the left panel of Fig. 7 where we plot μ_{DCC} vs μ_{Sch} , i.e. the distance moduli as computed from the $L_X - T_a$ and the other 2D correlations, respectively. Although with a large scatter, the data are consistent with a linear relation with slope 1, as it is also demonstrated by the right panel where μ_{DCC}/μ_{Sch} is next to 1 within 5% for all the points, but two (the only marginally deviant cases being GRB 050603 and GRB 060115). Averaging over the 17 GRBs, we find $\mu_{DCC}/\mu_{Sch} = 1.01 \pm 0.03$ with $(\mu_{DCC}/\mu_{Sch})_{rms} = 1.01$ and no correlation with redshift. As a further test, a linear regression (not weighting the points with their errors) gives:

$$\mu_{DCC} = (0.9 \pm 0.3)\mu_{Sch} + (5.5 \pm 13.5)$$

so that the slope is indeed consistent with 1. The small number of objects and the large intrinsic scatter makes the errors on the coefficient extremely large so that the offset detected is fully devoided of any statistical meaning. However, that such an offset is not present is also suggested by noting that $\langle \mu_{Sch} - \mu_{DCC} \rangle = -0.35 \pm 1.3$ so that indeed not statistically meaningful systematic offset is detected. Repeating the same linear fit but excluding the two points with $\mu_{DCC}/\mu_{Sch} > 1.05$ gives:

$$\mu_{DCC} = (1.2 \pm 0.3)\mu_{Sch} + (-8.6 \pm 12.2),$$

$$\langle \mu_{Sch} - \mu_{DCC} \rangle = -0.02 \pm 1.03,$$

thus showing that they are not biasing the comparison.

We therefore conclude that the use of the $L_X - T_a$ correlation does not introduce any bias and hence can be invoked to increase the number of GRBs in the fiducial HD. On the other hand, should future data disprove the $L_X - T_a$ correlation, one should reject from the fiducial HD the 14 GRBs

[§] Note that, here, we only refer to the fiducial GRBs HD since, as explained before, the local regression calibration of the $L_X - T_a$ correlation is not possible so that this 2D law has not been used in the derivation of the calibrated HD.

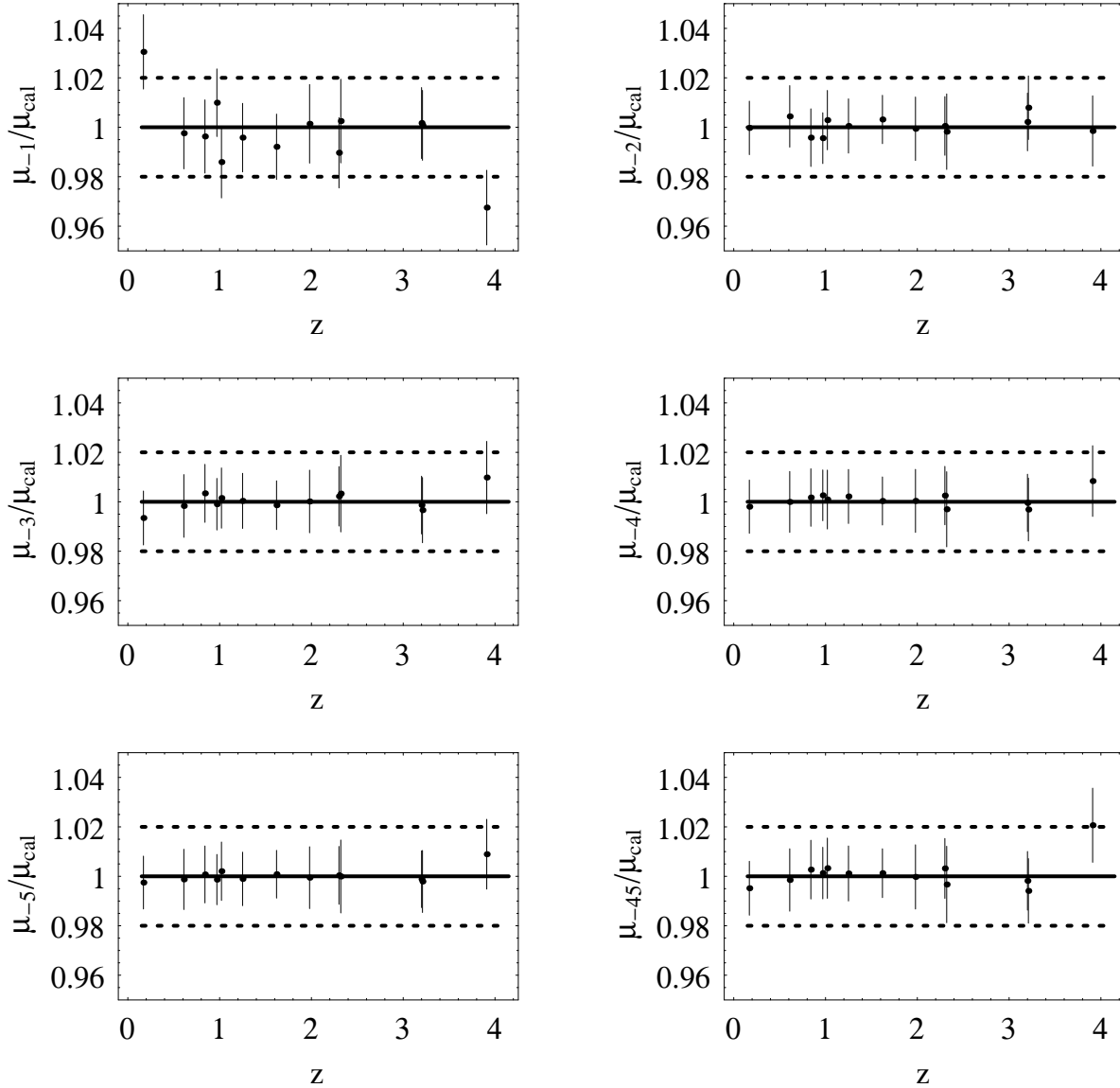


Figure 8. The ratio among the μ_{-i} and μ_{cal} values with μ_{-i} defined in the text and μ_{cal} the calibrated distance modulus.

having μ determined by this empirical law only so that one gets back the Schaefer Hubble diagram.

5.2 How many correlations ?

Although a lot of attention has been devoted recently to look for empirical correlations among GRB properties, it is still not clear whether the 2D laws we have used here are actually all real correlations or a consequence of different observational selection effects. Moreover, it is worth noting that five of them involve a luminosity measurement (the bolometric one, L , or the X-ray one, L_X) and three of them rely on a time measurement (being either τ_{lag} , τ_{RT} or T_a) so that one should also investigate whether they are actually independent relations. Investigating this issue in detail is outside our aims here, but we can nevertheless estimate what should be the impact of giving off one of the relations.

To this end, we consider the calibrated[¶] HD and select the 13 GRBs having μ estimated by all the canonical five correlations. We then denote with μ_{-i} the value of μ obtained by excluding the correlation i with $i = 1, \dots, 5$ for the $E_\gamma - E_p$, $L - E_p$, $L - \tau_{lag}$, $L - \tau_{RT}$ and $L - V$ respectively. We also denote by μ_{-45} the value obtained by excluding the $L - \tau_{RT}$ and $L - V$ correlations since they are those with the largest intrinsic scatter. Fig. 8 shows that the ratios μ_{-i}/μ_{cal} (with μ_{cal} the value reported in the HD) is very close to 1, with only two points deviating more than 4% from unity. Moreover, there is no apparent differences between the different panels and no trend with the redshift or the distance mod-

[¶] We prefer to use the calibrated rather than the fiducial HD in order to minimize the impact of choosing a cosmological model to determine the parameters of each correlation.

ulus. Although a more quantitative analysis with a larger number of objects is needed to draw a definitive answer, we may, however, argue from this preliminary analysis that the exclusion of one or two correlations does not alter the results. Put in other words, should one of the canonical 2D laws employed to get the calibrated HD be dismissed because of future evidences, we should not be afraid of any bias in the derived distance moduli.

5.3 The high z GRBs

Our sample includes 3 GRBs with $z > 5$, namely 060522 at $z = 5.11$, 050904 at $z = 6.29$ and 060116 at $z = 6.60$. As is apparent from Fig. 1, there is a clear gap between the two $z > 6$ GRBs and the rest of the sample so that one could wonder whether these two objects share the same properties of the other GRBs.

Actually, even if extreme in redshift, both 050904 and 060522 follow quite well the correlations they are involved in. In particular, 050904 does not deviate from five 2D laws, while the observed properties of 060522 make this object in good agreement with three 2D correlations. As such, we do not expect they bias anyway the fiducial HD. Moreover, being at such a high redshift, they are not used in the calibration of the 2D empirical laws based on the local regression analysis. Nevertheless, their distance moduli in the fiducial and calibrated HDs are in very good agreement. We therefore conclude that, notwithstanding the doubts on the validity of the 2D correlations at very high z , the inclusion of these two GRBs does not bias anyway the results.

5.4 Selection effects

Since the first works on the existence of correlations among GRBs properties allowing to use these objects as standardize candles, serious doubts were raised on the actual validity of such relations. Although being very luminous, the detection of GRBs is a complicated task so that different biases may favour the detection of a particular class of GRBs. Should this be indeed the case, one could argue that the 2D empirical laws are not universal or, what is worst, they only come out as a consequence of a detection bias (see, e.g., Butler et al. 2007 and Shahmoradi & Nemiroff 2009).

One possible example is represented by the shape of the GRB spectrum in the high energy region. GRBs more fluent at high energies (in their rest frame) at high redshift will be more likely to trigger local satellites since their energy is redshifted in the satellite bandpass. Approximating the energy spectrum as a power-law, i.e. $N(E) \propto E^{-\beta_{hr}}$ for large E , according to this scheme, high z GRBs with more shallow profiles will likely be detected preferentially over the steeper one. As a consequence, a plot of β_{hr} vs z should detect no correlation even if this is present. Schaefer (2007) reports the values of β_{hr} for 28 of the 69 GRBs in the calibrated HD, showing that there is indeed no variation with the redshift. For instance, roughly averaging over the 28 GRBs with measured β_{hr} , we find $\langle \beta_{hr} \rangle = -2.42$, while averaging over only the 17 GRBs with $z \leq 1.4$ gives $\langle \beta_{hr} \rangle = -2.47$. Note, however, that both distributions are quite asymmetric with most of the GRBs having $\beta_{hr} \geq -2.7$ and only 3 with $\beta_{hr} \leq -3$. It is also worth noting that, taken at face values, we find a

clear correlation between $\log L$ and β_{hr} with $\log L$ increasing with β_{hr} , although the large errors on β_{hr} prevents from deeming as statistically significant such a trend.

Quantifying the effect of a selection effect on β_{hr} would need the values of this parameter for all the GRBs in the sample which is not the case. However, since β_{hr} and $\log L$ are positively correlated, one can argue that selecting only GRBs with small $|\beta_{hr}|$ is the same as selecting those with the larger values of $\log L$ so that we can try investigating the effects of a possible selection on $\log L$ as an alternative approach. Rather than implementing a procedure based on the construction of mock samples (which would also need the details of the detection strategies of the different satellites), we make an ideal experiment using the GRBs in our sample. As a first step, we select only the GRBs with $z \leq 1.4$ and divide them in three samples referred to as CalAll, Cal51 and Cal52 containing all the GRBs with $\log L \geq \lambda$ with $\lambda = 0, 51, 52$ respectively^{||}. Using these samples, we recalibrate the five 2D correlations using the local regression method described in Sect. 4.2. We now use these calibrated relations to infer the GRBs distance moduli whatever the value of $\log L$ is thus simulating the case of an unknown selection effect on $\log L$ being at work. Comparing the distance moduli thus obtained, we find:

$$\mu_{Cal51} = (1.00 \pm 0.03) \mu_{CalAll} + (-0.1 \pm 1.3),$$

$$\mu_{Cal52} = (0.93 \pm 0.06) \mu_{CalAll} + (-2.6 \pm 2.7),$$

while for the offset we find:

$$\langle \mu_{Cal51} - \mu_{CalAll} \rangle = 0.29 \pm 0.44,$$

$$\langle \mu_{Cal52} - \mu_{CalAll} \rangle = 0.76 \pm 0.91.$$

It is worth stressing that the above linear fit has been done without taking into account the errors on the variables thus giving all the points the same weight. However, this qualitative analysis shows that, if a selection on $\log L$ should be at work, neglecting its effect does not bias the derived distance moduli in a statistically meaningful way. On the other hand, there is actually an increase in $\Delta\mu$ as λ increases thus motivating further and more quantitative investigation on this issue through a careful set of simulations.

6 GRBS HDS AS A DARK ENERGY PROBE

The search for standard candles has been always motivated by the need of building up reliable Hubble diagrams in order to probe the evolution of the universe. As Eqs.(16) and (20) clearly show, the Hubble diagram allows to estimate the luminosity distance as a function of redshift and put constraints on the integrated Hubble parameter $H(z)$ and hence on the cosmological parameters of a given model.

The importance of SNeIa for such a project is impossible to underrate as it is witnessed by the discovery of the cosmic speed up and the overwhelming flood of papers using this dataset to test the viability of different cosmological models. However, their main limitation is intimately related

^{||} Actually, the CalAll and Cal51 samples are almost identical, but we have preferred to not further divide the sample because of too low statistics.

to their nature preventing us from detecting SNeIa to redshift higher than $z \sim 2$. Moreover, even with future satellite missions, the most of the sample will be made out of objects with $z \leq 1$. As such, while they are excellent probes over the range $(0, 1)$ following the transition from the dark energy dominated present day universe to a decelerating expansion, SNeIa are unable to test the universe during the matter dominated era at $z \geq 2$. On the contrary, GRBs are ideal tools to probe the high redshift universe. That GRBs and SNeIa are complementary may be easily understood by considering, for instance, the redshift distribution of the nowadays sample. Indeed, while SNeIa mainly covers the range $(0, 1)$, GRBs are observed up to $z \sim 6.6$ with most of them lying at $z \geq 1$. As such, one may anticipate that they are less sensitive to the details of the dark energy EoS since they mainly probe the high z regime deep in the matter dominated era. It is this peculiar feature, opposite to what happens for SNeIa, that makes them a combined SNeIa+GRBs Hubble diagram an ideal tool to constrain the universe expansion.

6.1 Present day data

In order to show the power of a combined SNeIa + GRBs HD as a cosmological probe, we present here a first analysis fitting this dataset to two popular models, namely the Λ CDM and CPL EoS. For both cases, the scaled Hubble parameter $E(z) = H(z)/H_0$ is given by Eq.(21 with the Λ CDM being obtained by setting $(w_0, w_a) = (-1, 0)$. In order to constrain the model parameters, we maximize the following likelihood function :

$$\mathcal{L}(\mathbf{p}) \propto \exp(-\chi^2/2), \quad (23)$$

with

$$\begin{aligned} \chi^2(\mathbf{p}) = & \sum_{i=1}^{\mathcal{N}_{SNeIa}} \left[\frac{\mu_{obs}(z_i) - \mu_{th}(z_i, \mathbf{p})}{\sigma_i} \right]^2 \\ & + \sum_{i=1}^{\mathcal{N}_{GRB}} \left[\frac{\mu_{obs}(z_i) - \mu_{th}(z_i, \mathbf{p})}{\sqrt{\sigma_i^2 + \sigma_{int}^2}} \right]^2 \\ & + \left(\frac{h - h_{HST}}{\sigma_{HST}} \right)^2 + \left(\frac{\omega_M - \omega_M^{CMBR}}{\sigma_M} \right)^2. \end{aligned} \quad (24)$$

In Eq.(24), μ_{obs} and μ_{th} are the observed and theoretically predicted values of the distance modulus given the set of model parameters \mathbf{p} , while the sum is over the $\mathcal{N}_{SNeIa} = 307$ SNeIa in the Union dataset and the $\mathcal{N}_{GRB} = 69$ GRBs in the calibrated HD. Note that, for GRBs, we have added to the denominator the constant error parameter σ_{int} to take into account the intrinsic scatter^{**} around the Hubble diagram due to the scatter in the 2D correlations. The last two terms in Eq.(24) are Gaussian priors on h and $\omega_M = \Omega_M h^2$ and are included in order to help breaking the degeneracy with the other model parameters. To this aim, we resort to the result of the HST Key project (Freedman et al. 2001) to set $(h_{HST}, \sigma_{HST}) = (0.72, 0.08)$ and to the WMAP5 constraints

^{**} Note that a similar term is also present for SNeIa, but it is estimated to be $\sigma_{int} = 0.15$ and yet included into the error σ_i provided in the dataset.

(Dunkley et al. 2008) giving $(\omega_M^{CMBR}, \sigma_M) = (0.138, 0.004)$. Note that we have not added further data from other probes since we are here more interested in testing the ability of the combined HD to probe models rather than setting strong constraints on the model themselves (which will be the subject of a forthcoming publication).

In order to efficiently explore the parameter space, we run a Markov Chain Monte Carlo code generating chains with more than 100000 points which are enough to reach convergence. We then cut out the first 30% of the chains to avoid the burn in phase and thinned the chains taking one point each ten points in order to reduce fake correlations. For the Λ CDM model, we find for the best fit parameters :

$$(\Omega_M, h, \sigma_{int}) = (0.283, 0.701, 0.44)$$

giving

$$\chi_{SNeIa}^2/d.o.f. = 1.03 \quad , \quad \chi_{GRB}^2/d.o.f. = 1.11 \quad , \quad \omega_M = 0.139$$

with $d.o.f. = \mathcal{N}_{data} - \mathcal{N}_p$ and $\mathcal{N}_p = 3$ for the Λ CDM case. The reduced χ^2 close to 1 for both the SNeIa and GRB datasets and the very good agreement with the WMAP5 ω_M value clearly shows that the concordance Λ CDM model still stands out as an excellent description of the universe expansion. After marginalizing over the other quantities, the constraints on the model parameters are found to be :

$$\Omega_M = 0.287_{-0.013}^{+0.013} \quad {}_{-0.029}^{+0.027},$$

$$h = 0.700_{-0.006}^{+0.006} \quad {}_{-0.012}^{+0.012},$$

$$\sigma_{int} = 0.15_{-0.11}^{+0.21} \quad {}_{-0.13}^{+0.40},$$

where, following the Bayesian prescription, we give the median as central value and the reported errors refer to the 68 and 95% CL. It is worth noting that the constraints on σ_{int} shows that this quantity is weakly constrained with the median values being very different from the best fit one. This is, however, not surprising. On the one hand, it is well known that, because of degeneracies and projection effects, the maximum of $\mathcal{L}(\mathbf{p})$ is not given by the median values of the parameters. This could be the case only if the covariance matrix of the parameters is diagonal which is quite unusual. On the other hand, we have not included in the likelihood definition any prior on σ_{int} which could be inferred considering the intrinsic scatter of the 2D correlations used to build the GRB HD. Moreover, the asymmetry in the σ_{int} CL is a result of the obvious constraint that this quantity must be positive because of its same definition.

As a further example, we now consider the CPL case leaving the parameters (w_0, w_a) free in the fit thus giving $\mathcal{N}_p = 5$. For the best fit, we find :

$$(\Omega_M, w_0, w_a, h, \sigma_{int}) = (0.273, -1.28, 2.02, 0.707, 0.45)$$

giving

$$\chi_{SNeIa}^2/d.o.f. = 1.03 \quad , \quad \chi_{GRB}^2/d.o.f. = 1.06 \quad , \quad \omega_M = 0.136$$

so that there is still a perfect agreement with the data. Note that, formally, the CPL model fits the GRB data better than the Λ CDM one, but the increase by two of the number of parameters is actually not compensated by a corresponding reduction of the reduced χ_{GRB}^2 so that a pure cosmological constant is still preferred. One could be surprised that the best fit parameters seem to favour a model which is very

different from the Λ CDM one with the present day value of the EoS deep in the phantom regime $w_0 < -1$ and a strongly varying EoS. However, this is just a consequence of the parameter degeneracies quoted above^{††}. Indeed, the Bayesian constraints turn out to be:

$$\Omega_M = 0.283_{-0.022}^{+0.021} \quad {}_{-0.039}^{+0.036},$$

$$w_0 = -1.06_{-0.21}^{+0.19} \quad {}_{-0.42}^{+0.34},$$

$$w_a = 0.8_{-1.1}^{+0.8} \quad {}_{-1.9}^{+1.8},$$

$$h = 0.699_{-0.013}^{+0.016} \quad {}_{-0.022}^{+0.029},$$

$$\sigma_{int} = 0.08_{-0.05}^{+0.15} \quad {}_{-0.07}^{+0.42},$$

showing that the Λ CDM model with $(w_0, w_a) = (-1, 0)$ is well within the 68% CL. It is worth noting that the constraints on both w_0 and w_a are quite weak, as those on the intrinsic scatter σ_{int} . This same result is obtained if one only uses the SNeIa HD so that one could wonder whether adding the GRB data have improved the situation. Actually, this is not because, as we have yet quoted above, the GRBs HD only probes the matter dominated era when the dark energy term is almost disappeared so that the precise values of (w_0, w_a) are meaningless. As we will see later, GRBs improve, on the other hand, the constraints on Ω_M even if this is not apparent for the fits we are considering here because of the addition of the priors on h and ω_M . As a final remark, we note that, even with these weak constraints, we can exclude with high confidence historically discussed cosmological models with, e.g., $(\Omega_M, \Omega_\Lambda) = (1, 0)$ or $(\Omega_M, \Omega_\Lambda) = (0.3, 0)$, and have a further strong evidence for an accelerating universe.

6.2 Future SNeIa + GRB data

The analysis of the present day data have not shown the full complementarity between SNeIa and GRBs, essentially because we have added the priors on the two parameters h and ω_M . To better investigate this issue, we compute the Fisher information matrix (see, e.g., Tegmark et al. 1997 and references therein) defined as:

$$F_{ij} = \left\langle \frac{\partial^2 L}{\partial p_i \partial p_j} \right\rangle \quad (25)$$

with $L = -2 \ln \mathcal{L}(\mathbf{p})$, and we redefine the likelihood as in Eq.(23), but excluding the two priors on (h, ω_M) . Note that $\langle \dots \rangle$ denotes the expectation value, but, actually, this is computed by evaluating the Fisher matrix elements for fiducial values of \mathbf{p} . The inverse of the Fisher matrix gives the covariance matrix \mathbf{C} so that $\sigma_i = \sqrt{C_{ii}}$ is an estimate of the error on the parameter i . We remember that, because of the Cramer-Rao theorem, this is an upper limit on the error on the parameter p_i that can be obtained by an experiment with the given characteristics.

A key ingredient in the computation of \mathbf{F} is represented by the details of the SNeIa and GRB surveys giving the redshift distribution of the samples and the errors on each

measurement. For SNeIa, following Kim et al. (2004), we adopt^{††}:

$$\sigma(z) = \sqrt{\sigma_{sys}^2 + \left(\frac{z}{z_{max}}\right)^2 \sigma_m^2}$$

with z_{max} the maximum redshift of the survey, σ_{sys} an irreducible scatter in the SNeIa distance modulus and σ_m to be assigned depending on the photometric accuracy. For GRBs, we assume that the redshift distribution is provided is the same as the star formation history in Porciani & Madau (2001) although it is worth noting that this just a first order approximation. Indeed, one should convolve this theoretical distribution with the detection efficiency of a satellite, like *Swift* or *Fermi*, which will also claim for a model of GRB explosion to compute the expected fluence. Since all these quantities are up to know largely uncertain, we prefer to not detail them warning the reader that our results are somewhat optimistic. Concerning the error distribution, we assume that the main source of error is the intrinsic scatter (as it is indeed the case with the present day data) so that we give to each GRBs distance modulus an uncertainty randomly generated from a Gaussian centred on σ_{GRB} and with standard deviation σ_{std} . To further concentrate our attention on the constraints on the cosmological parameters, we moreover assume that the intrinsic scatter σ_{int} in Eq.(24) has been estimated somewhat and included in the error on μ so that this is no more a quantity to be constrained. Finally, in order to run the Fisher matrix calculation, we have to choose a fiducial model which we do by setting $(\Omega_M, w_0, w_a, h) = (0.277, -1, 0, 0.72)$ in agreement with the WMAP5 results.

As a first test, we consider the present day data thus using the observed redshift distribution as the Union one for SNeIa and that of the calibrated HD for GRBs. We further set $(\mathcal{N}_{SNeIa}, \sigma_m) = (307, 0.33)$ and $(\sigma_{GRB}, \sigma_{STD}) = (0.58, 0.22)$. With these values, we get:

$$\sigma(\Omega_M) = 0.58 \quad , \quad \sigma(w_0) = 0.17 \quad , \quad \sigma(w_a) = 1.2 \quad ,$$

using SNeIa data only, while adding GRBs gives:

$$\sigma(\Omega_M) = 0.08 \quad , \quad \sigma(w_0) = 0.08 \quad , \quad \sigma(w_a) = 0.4 \quad .$$

Such a test immediately shows the complementarity of SNeIa and GRBs with these latter data halving the error on Ω_M thanks to their ability of probing the matter dominated era. Note also the reduction of the errors on (w_0, w_a) which seems to contradict our claim that GRBs are not sensitive to the dark energy EoS. Actually, the reduction is due mainly to GRBs increasing the statistics rather than probing the EoS as is better understood considering future data.

To this end, we now simulate a SNAP-like SNeIa survey setting $(\mathcal{N}_{SNeIa}, \sigma_m) = (2000, 0.02)$ and using the Porciani & Madau (2001) distribution to generate 200 GRBs leaving the error parameters $(\sigma_{GRB}, \sigma_{std})$ unchanged. Using only SNAP SNeIa, we get:

$$\sigma(\Omega_M) = 0.077 \quad , \quad \sigma(w_0) = 0.039 \quad , \quad \sigma(w_a) = 0.22 \quad ,$$

^{††} Note also that we have not set here the usual prior $w_0 + w_a = 0$ which is typically introduced to assure that the dark energy EoS fades away in the early universe.

^{††} Note that, in Kim et al. (2004), the authors assume the data are separated in redshift bins so that the error becomes $\sigma^2 = \sigma_{sys}^2 / \mathcal{N}_{bin} + \mathcal{N}_{bin} (z/z_{max})^2 \sigma_m^2$ with \mathcal{N}_{bin} the number of SNeIa in a bin. However, we prefer to not bin the data so that $\mathcal{N}_{bin} = 1$.

while adding GRBs gives :

$$\sigma(\Omega_M) = 0.019 \quad , \quad \sigma(w_0) = 0.036 \quad , \quad \sigma(w_a) = 0.20 \quad .$$

The role of the complementarity of SNeIa and GRBs is now better explained. Indeed, while $\sigma(\Omega_M)$ is reduced by a factor ~ 4 , both $\sigma(w_0)$ and $\sigma(w_a)$ are almost unaltered by the addition of GRBs in agreement with the claim that their Hubble diagram is unable to put constraints on (w_0, w_a) .

As a final remark, it is worth noting that the detection of 200 GRBs is likely well within the capabilities of both the *Swift* and *Fermi* satellites so that one can argue that, by the time the SNAP survey will be completed, one indeed has the opportunity to build up a combined SNeIa + GRB HD as the one assumed in our Fisher matrix forecast. However, it is worth stressing that the precision attainable with GRBs may critically depend on their assumed redshift distribution and on the intrinsic scatter of the 2D correlations used to build up the calibrated HD. Both these key ingredients have been modelled very roughly in our analysis so that a more careful investigation should be needed. Although such a work can downgrade our optimistic forecast, we argue that similar results can still be obtained by increasing the number of GRBs still remaining within the realm of the *Fermi* satellite detection capabilities.

7 CONCLUSIONS

As soon as the need to probe the Hubble diagram to a redshift higher than the one attainable with SNeIa became clear, most attention has been devoted to search for a method to make GRBs standardizeable candles. To this aim, different 2D correlations between a luminosity or energy distance dependent quantity and observationally accessible GRBs properties have been proposed in order to build up a GRBs Hubble diagram to be used for constraining cosmological parameters. In an attempt to make a step forward along this road, we have here reconsidered different aspects of the problem trying with the final aim of constructing a more reliable GRBs Hubble diagram.

First, we have added the recently found $L_X - T_a$ correlation to the other five 2D empirical laws used up to now. Although being different from the other ones since it is based on afterglow rather than peak quantities, we have shown that the estimated distance modulus for each of the GRBs common to the Schaefer (2007) and Willingale et al. (2007) samples is in agreement with the one obtained using the standard set of 2D correlations. As such, one can be confident that no systematic bias is introduced by resorting to this new empirical law. On the contrary, its use makes it possible to both reduce the errors on $\mu(z)$ by a significant $\sim 14\%$ and increase the sample from 69 to 83 GRBs. With the *Swift* satellite still operating and collecting data on the X-ray afterglow, the prospects to both improve the estimate of the calibration parameters and adding still more GRBs to the sample are quite good. Needless to say, this is also possible for the peak based 2D correlations. It is worth noting that, in order to reduce the uncertainty on $\mu(z)$, following Schaefer (2007), we have made a weighted average of the estimates coming from the use of the six 2D correlations. While this makes it possible to, in a sense, average out any systematics intrinsic to each particular correlations,

such a procedure is not statistically well motivated. Actually, comparing the estimated $\mu(z)$ with each other and with the weighted average makes us confident that this method have not biased anyway the final results. However, increasing the sample will allow us to better cross check the results thus leading further confidence in this approach.

As a preliminary step in the construction of the GRBs HD, we have updated the calibration of the six 2D correlations we have used. To this aim, we have first to assume a background cosmological model to compute the distance dependent quantities. The recent WMAP5 data analysis has motivated our choice of a fiducial flat Λ CDM model with $(\Omega_M, h) = (0.291, 0.697)$, but we have also explored the effect of varying both (Ω_M, h) and the (w_0, w_a) parameters of the phenomenological CPL dark energy EoS. These data are then used as input to a Bayesian motivated fitting procedure which makes it possible to estimate both the slope a and the intrinsic scatter σ_{int} of the 2D correlations correctly taking into account the errors on both involved variables. To our knowledge, this is the first time that the 2D GRBs empirical laws have been calibrated using the same statistical tool for all of them. Moreover, our method avoids to underestimate the intrinsic scatter which plays an important role not only in the determination of the distance modulus uncertainty, but also in testing theoretical models of GRBs explosion and afterglow. As a somewhat surprising result, we find that the calibration parameters (a, b, σ_{int}) very weakly depend on the assumed cosmological model, i.e. on the value of (Ω_M, h, w_0, w_a) . As a consequence, the fiducial GRBs HD (i.e., the one relying on the calibrations made in the fiducial Λ CDM model) is essentially unaffected by varying the cosmology. Although this nice finding argues in favour of the use of the fiducial HD as a tool to constrain different cosmological models, we caution the reader that we have only explored a single class of dark energy theories. Indeed, the CPL parametrization makes it possible to mimic a quite large set of models, but may fail to mimic scenarios with a significant quantity of dark energy at high redshift. It is likely that the impact on (a, b, σ_{int}) is larger in this class of theories, even if it is worth stressing that they are disfavoured by the present dataset and the constraints from primordial nucleosynthesis.

In order to fully avoid the problem of assuming any background cosmology in the calibration procedure, we have illustrated a novel method relying on the estimate of the distance modulus of a given GRBs at redshift z through a local regression analysis of the Union SNeIa sample. As we have convincingly shown, local regression allows to recover the right value of $\mu(z)$ whatever are z and the parameters (Ω_M, h, w_0, w_a) of the underlying CPL cosmology. As a consequence, we can calibrate the 2D correlations using GRBs with $z \leq 1.4$ (i.e., overlapping the redshift range probed by SNeIa) without the need of assuming any fiducial cosmological model. This procedure finally leads us to what we term the calibrated GRBs HD containing 69 objects with model independent estimates of the distance modulus. Reassuringly, for the GRBs in common, the calibrated and fiducial HDs are in very good agreement thus suggesting that both of them are not affected by any systematic bias induced by the different calibration procedures.

One can wonder which is the GRBs HD better suited as a cosmological tool. This is somewhat a matter of personal

taste. Indeed, the two HDs agree in all of their properties also providing the same percentage of likely outliers with respect to a fiducial Λ CDM model. On one hand, the fiducial HD contains a larger number of objects with smaller uncertainties, but, although this is unlikely, one can still not exclude a bias originating from the model dependent calibration. On the other hand, the calibrated HD is free of any problem due to the unknown background cosmology, but its constraining power is likely to be weaker because of the lower number of objects and the greater uncertainties, both effects due to not having used the $L_X - T_a$ correlation. Should future data make it possible to calibrate also the $L_X - T_a$ law with the local regression based method, the calibrated HD should become as precise as the fiducial HD. As a concluding remark, we therefore argue in favour of this latter approach as the best way to use GRBs as cosmological tools.

ACKNOWLEDGEMENTS

We sincerely thank an anonymous referee for his/her comments which have helped to improve the paper. VFC is supported by Regione Piemonte and Università di Torino. Partial support from INFN project PD51 is acknowledged too.

APPENDIX A: HUBBLE DIAGRAMS DATA

As explained in the main text, the fiducial and calibrated HDs contain a different number of GRBs because it is not possible to use the local regression calibration for the $L_X - T_a$ relation. Therefore, we report in Table A1 the redshift and distance moduli of the 69 GRBs common to both samples, while Table A2 gives the same data for the 14 GRBs present only in the fiducial HD. Further material (such as the values of μ from the single 2D correlations) is available on request.

APPENDIX B: COMMENTS ON OUTLIERS

As we have quoted in Sect. 4.3, there are 13 (10) GRBs deviating more than 2σ from the fiducial (calibrated) HD which are therefore likely outliers. Actually, dealing with *likely outliers* is a complicated task since one has to find a serious motivation before rejecting a given object from a sample. To this end, one should look both at its eventually peculiar features and the instrumental and observing setup which has been used to gather the corresponding data. Since we have no access to these informations for all GRBs, we have preferred to not reject them.

Nonetheless, as an example, we discuss here the case of GRB 060614 which is the only GRB deviating more than 3σ from both the fiducial HD and the $L_X - T_a$ correlation. Indeed, this object is somewhat very peculiar being the first long GRB observed at low redshift ($z = 0.125$) and clearly not associated to a bright Ib/c SN (Della Valle et al. 2006). Actually, its short duration ($T_{90} = 100$ s) makes it hardly classifiable as a long GRB, while its morphology is quite similar to the one of GRB 0507024 which is indeed classified as a short GRB (Piro 2005; Zhang et al. 2007). It is worth noting that GRB 060614 has been interpreted both in the framework of the canonical fireshell model (Ruffini et al. 2001; Caito et al. 2008) and by (Norris & Bonnell 2006) as

Table A1. Fiducial and calibrated Hubble diagrams data for the 69 GRBs common to both samples. Order of the columns as follows: 1. GRBs id; 2. redshift; 3., 4. distance moduli (with 1σ error) from the fiducial and calibrated HDs.

Id	z	μ_{fid}	μ_{cal}
970228	0.70	43.04 ± 0.68	42.72 ± 0.68
970508	0.84	43.79 ± 0.44	43.76 ± 0.35
979828	0.96	43.38 ± 0.49	43.07 ± 0.38
971214	3.42	47.77 ± 0.59	47.54 ± 0.59
980613	1.10	44.93 ± 1.29	44.75 ± 1.22
980703	0.97	44.16 ± 0.42	43.84 ± 0.32
990123	1.61	44.36 ± 0.47	44.66 ± 0.37
990506	1.31	43.94 ± 0.56	43.76 ± 0.53
990510	1.62	45.31 ± 0.42	45.36 ± 0.31
990705	0.84	43.72 ± 0.49	43.40 ± 0.38
990712	0.43	41.96 ± 0.62	41.76 ± 0.44
991208	0.71	41.87 ± 0.66	41.65 ± 0.65
991216	1.02	42.95 ± 0.44	43.12 ± 0.35
000131	4.50	47.21 ± 0.68	47.14 ± 0.68
000210	0.85	42.34 ± 0.66	42.27 ± 0.65
000911	1.06	44.21 ± 0.68	44.27 ± 0.67
000926	2.07	45.39 ± 0.69	45.09 ± 0.68
010222	1.48	43.98 ± 0.46	44.62 ± 0.29
010921	0.45	43.00 ± 0.58	42.53 ± 0.54
011211	2.14	45.77 ± 0.62	45.53 ± 0.43
020124	3.20	46.88 ± 0.45	46.73 ± 0.37
020405	0.70	43.48 ± 0.52	43.47 ± 0.46
020813	1.25	44.07 ± 0.43	43.95 ± 0.33
020903	0.25	43.07 ± 1.26	42.23 ± 1.16
021004	2.32	46.81 ± 0.52	46.60 ± 0.48
021211	1.01	43.94 ± 0.61	43.49 ± 0.55
030115	2.50	46.60 ± 0.59	46.25 ± 0.57
030226	1.98	46.66 ± 0.48	46.50 ± 0.40
030323	3.37	47.79 ± 0.97	47.65 ± 0.96
030328	1.52	44.80 ± 0.50	44.68 ± 0.37
030329	0.17	40.56 ± 0.42	39.73 ± 0.29
030429	2.66	46.80 ± 0.58	46.61 ± 0.53
030528	0.78	45.12 ± 0.58	44.31 ± 0.54
040924	0.86	44.06 ± 0.61	43.61 ± 0.55
041006	0.71	44.03 ± 0.50	43.92 ± 0.42
050126	1.29	46.33 ± 0.55	45.74 ± 0.52
050318	1.44	46.09 ± 0.51	45.95 ± 0.44
050319	3.24	47.53 ± 0.66	47.73 ± 0.93
050401	2.90	46.15 ± 0.53	45.94 ± 0.55
050406	2.44	48.44 ± 0.72	48.03 ± 0.70
050408	1.24	45.52 ± 0.76	45.09 ± 0.72
050416	0.65	43.98 ± 0.85	43.32 ± 0.81
050502	3.79	47.51 ± 0.63	47.24 ± 0.64
050505	4.27	48.47 ± 0.55	48.49 ± 0.59
050525	0.61	43.55 ± 0.44	43.28 ± 0.37
050603	2.82	45.12 ± 0.55	44.66 ± 0.58
050802	1.71	45.50 ± 0.66	45.52 ± 0.98
050820	2.61	46.51 ± 0.63	46.27 ± 0.59
050824	0.83	44.65 ± 1.19	44.07 ± 1.19
050904	6.29	48.86 ± 0.52	49.27 ± 0.47
050908	3.35	47.38 ± 0.76	47.00 ± 0.76
050922	2.20	45.71 ± 0.55	45.57 ± 0.52
051022	0.80	43.61 ± 0.46	43.77 ± 0.28
051109	2.35	45.87 ± 0.83	45.84 ± 0.80
051111	1.55	45.14 ± 0.63	44.54 ± 0.60

Table A1 – *continued*

Id	z	μ_{fid}	μ_{cal}
060108	2.03	47.93 ± 0.72	48.85 ± 1.07
060115	3.53	48.21 ± 0.80	47.78 ± 0.79
060116	6.60	48.67 ± 0.77	48.33 ± 0.92
060124	2.30	46.35 ± 0.40	46.78 ± 0.38
060206	4.05	46.55 ± 0.51	46.37 ± 0.60
060210	3.91	48.30 ± 0.45	48.59 ± 0.47
060223	4.41	47.94 ± 0.57	47.64 ± 0.54
060418	1.49	45.09 ± 0.47	45.00 ± 0.51
060502	1.51	45.37 ± 0.65	44.90 ± 0.62
060510	4.90	48.66 ± 0.94	48.60 ± 0.93
060526	3.21	47.56 ± 0.43	47.17 ± 0.41
060604	2.68	47.18 ± 0.55	46.23 ± 0.57
060605	3.80	47.66 ± 0.57	47.04 ± 0.68
060607	3.08	46.68 ± 0.58	46.24 ± 0.55

Table A2. Hubble diagram data for the 14 GRBs present in the fiducial one only. Order of the columns as in Table A1.

Id	z	μ_{fid}
050315	1.95	46.11 ± 0.98
050416A	0.65	44.73 ± 1.14
050820A	2.61	45.43 ± 0.97
050922C	2.20	44.74 ± 0.98
051016B	0.94	42.81 ± 1.65
051109A	2.35	45.49 ± 1.17
060223A	4.41	50.09 ± 1.25
060502A	1.51	46.06 ± 1.36
060522	5.11	49.65 ± 1.10
060607A	3.08	49.43 ± 1.73
060614	0.12	42.26 ± 0.88
060707	3.43	48.12 ± 1.41
060714	2.71	45.41 ± 1.10
060729	0.54	42.55 ± 0.89

a new class of intermediate sources. All these peculiarities indeed argue in favour of the rejection of this GRB from the fiducial HD as a physical outlier.

Another interesting case is represented by GRB 060505 which is not associated by any SN thus suggesting it is representative of a class of objects with different progenitors. However, among the likely outliers, we also find GRB 030329 which is one of spectroscopically confirmed GRBs associated with a SN. However, its X-ray afterglow was observed with only two pointings of the Rossi-XTE instrument obtained respectively 5 hours and 1.24 days after the burst (Marshall & Swank 2003; Marshall et al. 2003). Actually, an incomplete coverage of the X-ray lightcurve typically takes place for many GRBs observed with the old missions such as Beppo SAX, Rossi, HETE2. One can argue that the parameters obtained in these cases are somewhat incorrectly estimated thus altering the position of the corresponding GRB in the fiducial HD. This could be the case for 10 out of 13 likely outliers GRBs (namely : 990123, 991208, 991216, 990506, 000210, 010222, 020813, 020903, 030329, 030528) thus suggesting that they could be rejected because of observationally (rather than physically) motivated problems. As it should be clear from these comments, we have up

to now only some phenomenological and qualitative hints to address the problem of outliers. We therefore deserve a detailed analysis also taking into account more quantitative features to a forthcoming publication.

REFERENCES

- Aldering, G., Althouse, W., Amanullah, R., Annis, J., Astier, P. et al., 2004, arXiv:astro-ph/0405232, see also `snap.1b1.gov`
- Astier, P., Guy, J., Regnault, N., Pain, R., Aubourg, E. et al. 2006, *A&A*, 447, 31
- Band, D., Matteson, J., Ford, L., Schaefer, B.L., Palmer, D. et al. 1993, *ApJ*, 413, 281
- Basilakos, S., Perivolaropoulos, L. 2008, *MNRAS*, 391, 411
- Bennett, C.L., Halpern, M., Hinshaw, G., Jarosik, N., Kogut, A. et al. 2003, *ApJS*, 148, 1
- Bloom, J.S., Frail, D.A., Sari, R. 2001, *AJ*, 121, 2879
- Bradley, S., 2003 *ApJ*, 583, L67
- Butler, N.R., Kocevski, D., Curtis, J.L., Bloom, J.S. 2007, *ApJ*, 671, 656
- Caito, L., Bernardini, M.G., Bianco, C.L., Dainotti, M.G., Guida, R., Ruffini, R. 2008, arXiv:0810:4855
- Capozziello, S., Cardone, V.F., Salzano, V. 2008, *Phys. Rev. D*, 78, 063504
- Capozziello, S., Izzo, L. 2008, *A&A*, 490, 31
- Carroll, S.M., Press, W.H., Turner, E.L. 1992, *ARAA*, 30, 499
- Chevallier, M., Polarski, D. 2001, *Int. J. Mod. Phys. D*, 10, 213
- Cleveland, W.S. 1979, *J. Amer. Stat. Ass.*, 74, 829
- Cleveland, W.S., Devlin, S.J. 1988, *J. Amer. Stat. Ass.*, 83, 596
- Copeland, E.J., Sami, M., Tsujikawa, S. 2006, *Int. J. Mod. Phys. D*, 15, 1753
- D'Agostini, G. 2005, arXiv:physics/051182
- Dai, Z.G., Liang, E.W., Xu, D. 2004, *ApJ*, 612, L101
- Dainotti, M.G., Cardone, V.F., Capozziello, S. 2008, *MNRAS*, 391, L79
- Daly, R.A., Djorgovski, S.G., Freeman, K.A., Mory, M.P., O'Dea, C.P., Kharb, P., Baum, S. 2008, *ApJ*, 677, 1
- Davis, T., Mörtzell, E., Sollerman, J., Becker, A.C., Blondin, S. et al. 2007, *ApJ*, 666, 716
- de Bernardis, P., Ade, P.A.R., Bock, J.J., Bond, J.R., Borrill, J. et al. 2000, *Nature*, 404, 955
- Della Valle, M., Chincarini, G., Panagia, N., Tagliaferri, G., Malesani, D. et al. 2006, *Nature*, 444, 1050
- Dodelson, S., Narayanan, V.K., Tegmark, M., Scranton, R., Budavari, T. et al. 2002, *ApJ*, 572, 140
- Dvali, G.R., Gabadadze, G., Porrati, M. 2000, *Phys. Lett. B*, 485, 208, 2000
- Dunkley, J., Komatsu, E., Nolte, M.R. et al. 2008, arXiv:0803.0568 [astro-ph]
- Eisenstein, D.J., Zehavi, I., Hogg, D.W., Scoccimarro, R., Blanton, M.R. et al. 2005, *ApJ*, 633, 560
- Femore, E.E., Ramirez-Ruiz, E. 2000, arXiv:
- Firmani C., Ghisellini, G., Ghirlanda, Avila-Reese, G. 2005, *MNRAS*, 360, L1
- Firmani C., Ghisellini, G., Avila-Reese, V., Ghirlanda, G. 2006, *MNRAS*, 372, L28
- Freedman, W.L., Madore, B.F., Gibson, B.K., Ferrarese, L., Kelson, D.D., Sakai, S., Mould, J.R.; Kennicutt, R.C. et al., *ApJ*, 553, 47, 2001
- Galama, T., Vreeswick, P.M., van Paradjis, J., Kouveliotou, C., Augusteijn, T. et al. 1998, *Nature*, 395, 670
- Ghirlanda, G., Ghisellini, G., Lazzati, D. 2004, *ApJ*, 616, 331
- Ghirlanda G., Ghisellini G. & Firmani C., 2006, *New Journal of Physics*, 8, 123
- Ghisellini G., Nardini, M., Ghirlanda, G., Celotti, A. 2008, arXiv:0811.1578

- Greiner, J., Kruehler, T., Fynbo, J.P.U., Rossi, A., Schwarz, R. et al. 2008, arXiv:0810.2314
- Hawkins, E., Maddox, S., Cole, S., Lahav, O., Madgwick, D.S. et al. 2003, MNRAS, 346, 78
- Kim, A.G., Linder, E.V., Miquel, R., Mostek, N. 2004, MNRAS, 347, 909
- Kodama, Y., Yonetoku, D., Murakami, T., Tanabe, S., Tsutsui, R., Nakamura, T. 2008, MNRAS, 391, L1
- Kowalski, M., Rubin, D., Aldering, G., Agostinho, R.J., Amadon, A. et al. 2008, arXiv:0804.4142 [astro-ph]
- Li, H., Su, M., Fan, Z., Dai, Z., Zhang, X. 2008, Phys. Lett. B, 658, 95
- Liang, E.W., Zhang, B. 2006, MNRAS, 369, L37
- Liang, N., Xiao, W.K., Liu, Y., Zhang, S.N. 2008, ApJ, 385, 654
- Linder, E.V. 2003, Phys. Rev. Lett., 90, 091301
- Loader, C. 1999, *Local regression and likelihood*, Springer - Verlag, New York
- Lue, A., Scoccimarro, R., Starkman, G. 2004, Phys. Rev. D, 69, 124015
- Marshall, F., Swank, J.H. 2003, GRB Coordinates Network, 1996, 1
- Marshall, F.E., Markwardt, C., Swank, J.H. 2003, GRB Coordinates Network, 2052, 1
- Norris, J.P., Marani, G.F., Bonnell, J.T. 2000, ApJ, 534, 248
- Norris, J.P., Bonnell, J.T. 2006, ApJ, 643, 266
- Padmanabhan, T. 2003, Phys. Rept., 380, 235, 2003
- Peebles, P.J.E., Rathra, B. 2003, Rev. Mod. Phys., 75, 559
- Percival, W.J., Sutherland, W., Peacock, J.A., Baugh, C.M., Hawthorn, J. et al. 2002, MNRAS, 337, 1068
- Percival, W.J., Cole, S., Eisenstein, D.J., Nichol, R.C., Peacock, J.A., Pope, A.C., Szalay, A.S. 2007, MNRAS, 381, 1053
- Perlmutter, S., Gabi, S., Goldhaber, G., Goobar, A., Groom, D.E. et al. 1997, ApJ, 483, 565
- Piro, L. 2005, Nature, 437, 822
- Porciani, C., Madau, P. 2001, ApJ, 548, 522
- Riechart, D.E., Lamb, D.Q., Fenimore, E.E., Ramirez-Ruiz, E., Cline, T.L. 2001, ApJ, 552, 57 2007
- Riess, A.G., Filippenko, A.V., Challis, P., Clocchiati, A., Diercks, A. et al. 1998, AJ, 116, 1009
- Riess, A.G., Strolger, L.G., Casertano, S., Ferguson, H.C., Mobasher, B. et al. 2007, ApJ, 659, 98
- Ruffini, R., Bianco, C.L., Frascchetti, F., Xue, S.S., Chardonnet, P. 2001, ApJ, 555, L113
- Sahni, V., Starobinski, A. 2000, Int. J. Mod. Phys. D, 9, 373
- Schaefer, B.E. 2003, ApJ, 583, L67
- Schaefer, B.E. 2007, ApJ, 660, 16
- Shahmorandi, A., Nemiroff, R.J. 2009, preprint, arXiv:0904.1464
- Spergel, D.N. et al. 2007, ApJS, 170, 377
- Sotiriou, T., Faraoni, V. 2008, arXiv:0805.1726 [astro-ph]
- Szalay, A.S. et al. 2003, ApJ, 591, 1
- Tegmark, M., Taylor, A.N., Heavens, A.F. 1997, ApJ, 480, 22
- Xu, D., Dai, Z.G., Liang, E.W. 2005, ApJ, 633, 603
- Yamazaki, R. 2008, arXiv:0810.1089
- Yonetoku, D., Murakami, T., Nakamura, T., Yamazaki, R., Inoue, A.K., Ioka, K. 2004, ApJ, 609, 935
- Wang, F.Y., Dai, Z.G., Zhu, Z.H. 2007, ApJ, 667, 1
- Wei, H., Zhang, S.N. 2008, arXiv:0808.2240 [astro-ph]
- Willingale, R.W., O'Brien, P.T., Osborne, J.P. et al. 2007, ApJ, 662, 1093
- Wood-Vasey, W.M., Miknaitis, G., Stubbs, C.W., Jha, S., Riess, A.G. et al. 2007, ApJ, 666, 694
- Wright, E.L. 2007, ApJ, 664, 633
- Zhang, B., Zhang, B.-B., Liang, E.-W., et al. 2007, ApJ, 655, L25